MATCH
Communications in Mathematical and in Computer Chemistry

MATCH Commun. Math. Comput. Chem. **92** (2024) 371–416
ISSN: 0340–6253
doi: 10.46793/match.92-2.371F

Bounds on Molecular Properties of π Systems: First-order Properties

Patrick W. Fowler, Barry T. Pickup

Department of Chemistry, University of Sheffield, Sheffield, S3 7HF, UK

P.W.Fowler@sheffield.ac.uk, B.T.Pickup@sheffield.ac.uk

(Received February 7, 2024)

Abstract

We derive upper and lower bounds to first-order properties in the Hückel model: π charge, bond order, bond number, and matrices of higher spectral moments. Bounds that depend on the electronic configuration, and on the molecular graph alone are derived. A ladder of relations between higher and lower spectral moments leads to bounds *via* the Cauchy-Schwarz theorem. The old square-root degree bound on bond number implicit in the work of Coulson, Moffitt and Longuet-Higgins is sharpened. Key to this development is the distinction between core and core-forbidden vertices of a graph.

1 Introduction

Simple models such as Hückel Theory give qualitative understanding of conjugated π systems in terms of ideal electron counts, location of strong and weak bonds, tendency of a π system to aromaticity or otherwise, site preferences for radical reactivity, and so on [8, 10–14]. Given their clear mathematical status in terms of adjacency matrices of graphs, it has been found of interest to derive rigorous bounds for chemically significant properties such as charge, bond order, bond number, and related spectral moments (at least within the assumptions of this simplified model) [15,20].

The bounds developed in the present paper link values of these basic properties to each other and to the graph properties of eigenvalues, eigenvectors, and shell invariants. It may be objected that once the graph is given, it is often as easy to calculate the properties themselves as to calculate the bounds, but this objection would miss the advantages of having a general overview.

For example, bond number was introduced as a proxy for the reactivity of a π-system [9], but also has interesting connections to energy and orbital energy. For an all-carbon framework, bond number, $N_{\rm r}$, determines the contribution of atom r to total π-energy. Placing electrons in a non-bonding orbital of such a framework may affect individual bond orders but leaves all bond numbers unchanged. In a sense, therefore, the bond number profile gives an alternative definition of what it means for a π system to have a non-bonding shell. The existence in principle of an upper bound for bond number is the crucial factor that allowed Coulson and his school to define *Free Valence* as a measure of the remaining capacity for bonding at a given site in a π system [5]. The history of the derivation of the bound is long and tortuous (as summarised in our paper [17] on proving 'Coulson's Lost Theorem'), but the bound itself is simple and informative: π bond number cannot exceed the square root of the vertex degree, and it reaches this value uniquely for the central vertex of a star graph [17]. Availability of this 'Coulson-Moffitt bound' motivates interesting connections with more recent developments in chemistry, *e.g.* conductivity of carbon nanotubes, and site reactivity in fullerenes.*

The structure of the paper is as follows. §2 to §5 review some basic definitions in Hückel theory, the standard approach to many-electron configurations, definition of the natural configuration, the notion of configuration state averages, and the definition of configuration state average properties. All our derived bounds refer to such averages, which are invariant under the symmetries of the underlying graph. §6 then introduces

*One observation, not mentioned in [17], is that Coulson's relationship between bond number and graph energy, E^G, together with McClelland's bound for graph energy [20,22], would already have given the $\sqrt{d_{\rm r}}$ bound on $N_{\rm r}$ for the class of vertex transitive (VT) graphs in their natural electronic configuration. For a VT graph: $\widetilde{N}_{\rm r} = E^G/n$ and McClelland gives $E^\pi \leq E^G \leq \sqrt{2mn}$, with $m = nd_{\rm r}/2$, hence $N_{\rm r} \leq \widetilde{N}_{\rm r} \leq \sqrt{d_{\rm r}}$. C_{60} is an example of a VT chemical graph.

general first order properties as matrix elements of spectral moments, leading to the ladder relations defined in §7. §8 discusses the special structure of these moments for bipartite graphs. Spectral moment matrix elements have generic property profiles as a function of electron number, and these are discussed in §9. The main theoretical results of the paper are contained in §10, which provides proofs of bounds of Gutman, Cauchy-Schwarz and non-configurational types, extending classical work by Coulson, Longuet-Higgins, Gutman and others. §11 gives detailed numerical results for some typical π-systems. The paper concludes with a summary of the main results as they apply to a π system in the natural configuration.

2 The Hückel model

The Hückel (tight-binding) model uses single atomic p_π basis functions, $\chi_{\rm r}$, on carbon centres, ${\rm r} = 1, \cdots, n$, to construct molecular orbitals (MOs) $\psi_{\rm k}$ as linear combinations

$$\psi_{\rm k} = \sum_{\rm k=1}^{n} {\rm U_{rk}} \chi_{\rm r}, \tag{1}$$

where the MOs form a unitary matrix $\mathbf{U}$ that diagonalises $\mathbf{H}^\pi$, the Hückel Hamiltonian matrix,

$$\sum_{\rm s=1}^{n} {\rm H^\pi_{rs}} {\rm U_{sk}} = {\rm U_{rk}} \epsilon_{\rm k}, \tag{2}$$

with $\epsilon_{\rm k}$ representing the orbital energy of the k-th MO. The Hamiltonian matrix has entries

$${\rm H^\pi_{rs}} = \begin{cases} \alpha_{\rm r} & \text{for r = s,} \\ \beta_{\rm rs} & \text{for r} \neq \text{s and r} \sim \text{s, } \textit{i.e.} \text{ r,s } \sigma \text{ bonded ,} \\ \beta_{\rm rs} = 0 & \text{for r} \neq \text{s and r} \not\sim \text{s } \textit{i.e.} \text{ r,s not } \sigma \text{ bonded,} \end{cases} \tag{3}$$

where $\alpha_{\rm r}$ and $\beta_{\rm rs}$ are Coulomb and resonance integrals, both negative energy quantities. In the simplest (all-carbon) case, we take $\alpha_{\rm r} = \alpha$ for all carbon centres, and $\beta_{\rm rs} = \beta$ for all σ-bonded pairs of centres and then the

Hamiltonian is related to the adjacency matrix of the unweighted graph, G, by

$$\mathbf{H}^{\pi} = \alpha\mathbf{1} + \beta\mathbf{A}, \tag{4}$$

where $\mathbf{A}$ is the adjacency matrix, with entries 1 for graph edges and 0 elsewhere. The π-system of a molecule can be seen as a graph in which vertices represent atomic centres and edges interactions between bonded atoms. The eigenvalues of $\mathbf{A}$ are (in non-increasing order): $\lambda_1 > \lambda_2 \geq \cdots \geq \lambda_n$. Molecular orbital (MO) energies are related to eigenvalues of $\mathbf{A}$ by

$$\epsilon_{\mathrm{k}} = \alpha + \lambda_{\mathrm{k}}\beta. \tag{5}$$

It is customary to define the energy scale such that α is zero, and to state all energies with respect to this origin as multiples of the negative energy, β. Positive, zero and negative eigenvalues in this system of units are associated with bonding, non-bonding and anti-bonding orbitals, respectively. The set of all orbitals of a given energy is said to form a *shell* (in mathematical terms, the eigenspace for the given eigenvalue). Systems with hetero-atoms can be included by introducing parameterised edge and vertex weights, *i.e.* effectively replacing the $\{0, 1\}$ matrix $\mathbf{A}$ in (4) with the adjacency matrix of a weighted graph,

$$\mathrm{A}_{\mathrm{rs}} = \begin{cases} (\alpha_{\mathrm{r}} - \alpha)/\beta \text{ for r} = \mathrm{s}, \\ \beta_{\mathrm{rs}}/\beta \text{ for r} \neq \mathrm{s}, \end{cases} \tag{6}$$

where α and β are the standard all-carbon values.

3 Electrons in many-electron configurations

As well known from basic courses in chemistry, the lowest energy (*ground*) electronic state of a system with a fixed number of electrons is obtained by placing them in orbitals according to three distinct rules:

1. *The Aufbau Principle:* Electrons are placed in the lowest available orbitals in order of increasing energy (*i.e.* in order of decreasing λ_{k}).

2. *The Pauli Principle:* Electrons have an extra degree of freedom: the spin. Electron spin is two-valued, and it is convenient to envisage the electron as of either *up* or *down* spin. Electrons are placed in the orbital of lowest energy until all spin states have been filled. Hence, an orbital may have occupancy, $n_{\rm k}$, of 0, 1, or the maximum of 2.

3. *Hund's Rule:* Spins of electrons in a degenerate shell in the ground state should be arranged, as far as possible, with parallel spins. We can ignore Hund's Rule in Hückel Theory, as this is a one-electron theory and it is the electron-electron repulsion that causes electron configurations with different spin arrangements to have different energies. The tendency of the rule to lead to an even spread of electrons through the shell is taken into account by using fractional occupation numbers. In shell J, of degeneracy $g_{\rm J}$, with eigenvalue $\lambda_{\rm J}$, containing $n_{\rm J} \leq 2g_{\rm J}$ electrons, the shell contribution to total π-energy in the Hückel model is $n_{\rm J}\lambda_{\rm J}$, irrespective of the spin pattern and occupancy of different eigenstates within that shell.

A configuration constructed using these rules is known as an *Aufbau configuration*, $\mathcal{C}_{\rm Auf}$,

In this work we consider trends in molecular properties in the Hückel model, as the number of electrons rises from 0 to the highest possible value for an n-vertex graph, namely $2n$. *Aufbau* electronic configurations, $\mathcal{C}_{\rm Auf}$, may possess an occupied shell of highest energy that is partially occupied. Such a configuration is an *open-shell* configuration. In the Hückel model, a molecule with an odd number of π electrons *must* have an open shell, even if the top occupied orbital is non-degenerate.

In quantum chemistry the term 'shell' is extended to include any group of orbitals with the same occupancy. We distinguish three such shells in terms of electronic occupation of their molecular orbitals (MOs). The closed shell, C, has all constituent MOs doubly occupied ($n_{\rm k} = 2$). The open shell, O, comprises a set of orbitals with single eigenvalue $\lambda_{\rm O}$, and degeneracy $g_{\rm O}$. The virtual shell, V, consists of all unoccupied MOs ($n_{\rm k} = 0$), *i.e.* all MOs not in C or O. Shell MOs ψ are defined so that their eigenvalues satisfy $\lambda_{\rm C} > \lambda_{\rm O} > \lambda_{\rm V}$, for all $\psi_{\rm C} \in$ C, $\psi_{\rm O} \in$ O, and $\psi_{\rm V} \in$ V. The

electronic configuration implied by these definitions is therefore an *Aufbau* configuration. The electronic occupation of the open shell, n_{O}, is less than the $2g_{\mathrm{O}}$ electrons that (allowing for spin) would make it doubly occupied. A potential problem with such partially occupied degenerate shells is that they are defined only to within a unitary transformation, whereas it is clear on physical grounds that properties such as the π-electron energy and the electron density cannot depend on a specific arbitrary choice of MOs.

Amongst all possible Aufbau configurations, each molecule possesses a *natural configuration*, $\mathcal{C}_{\mathrm{nat}}$. This is an *Aufbau* configuration such that shell C comprises *all* orbitals that have positive eigenvalues, and an open shell for which we adopt the special notation, K, consists of a half-occupied eigenspace with eigenvalue $\lambda_{\mathrm{O}} = 0$, if this eigenvalue is present, with common occupancy $\nu_{\mathrm{K}} = 1$. The eigenspace K with eigenvalue 0 is the nullspace or *kernel* of $\mathrm{A}(G)$. The degeneracy of the nullspace is the nullity, η. If the spectrum of the graph contains no zero eigenvalue, then the K shell is missing, and $\mathcal{C}_{\mathrm{nat}}$ is a closed-shell configuration. For highly electron-deficient/excessive molecules, the net charge implied by $\mathcal{C}_{\mathrm{nat}}$ can be large; in such cases Hückel theory must be applied with caution.

Occupation of the non-bonding orbitals is a key factor in chemical interpretation. To make this precise, we use the graph-theoretical notions of core vertex (CV) and core-forbidden vertex (CFV) [25, 26]. A vertex r is a CV if it has a non-zero coefficient, U_{rk}, for *some* non-trivial vector in the nullspace. Conversely, a vertex is a CFV if it has zero coefficients for *every* such vector. By extension, λ_{k}-CV and λ_{k}-CFV are defined with reference to their support in the eigenspace for λ_{k}.

4 Configuration State Averages

We can provide a description of a general open-shell configuration that is independent of the specific basis adopted for the open-shell MOs. The simplest such way of representing quantum mechanical properties for open-shell states is to use a *configuration state average*. The use of configuration state averages goes back to the earliest numerical quantum chemical work

on atoms by Hartree [19]. It circumvents the technical problems arising from the existence of open shells (states where a degenerate level is not fully occupied). Open-shell states give rise to the possibility of different electronic spin arrangements, some of which may have a subset of empty degenerate orbitals. Orbitals within a degenerate shell, however, are only defined up to a unitary transformation. The configurational state average approach takes an average over all possible electronic arrangements within an open shell, hence rendering the calculated properties invariant to any unitary transformation amongst the degenerate set of orbitals. By taking the average, we risk missing state-specific effects, such as Jahn-Teller distortion (which can be handled heuristically with weighted graphs [7]) and properties dependent on spin. This feature will require more detailed consideration when we treat second-order properties in a future work.

A configuration state average involves a sum over the expectation values for all possible states that can be formed by an open shell O of degeneracy g_{O} when the occupancy is

$$n_{\mathrm{O}} = \sum_{\mathrm{k}\in\mathrm{O}} n_{\mathrm{k}} < 2g_{\mathrm{O}}. \tag{7}$$

We will show that configuration state averages for first-order properties are represented by orbital contributions in which *each* orbital, $\psi_{\mathrm{k}}\in$O, in an open shell is weighted by the same fractional occupancy, ν_{O} (*c.f.* pp. 27-30 of [27]). The total number of electron configurations that obey the Pauli Principle is

$$M^{\mathrm{tot}} = \binom{2g_{\mathrm{O}}}{n_{\mathrm{O}}} = \frac{2g_{\mathrm{O}}}{n_{\mathrm{O}}}\binom{2g_{\mathrm{O}}-1}{n_{\mathrm{O}}-1}, \tag{8}$$

as the open shell can hold $2g_{\mathrm{O}}$ electrons in total. We now consider how many of these configurations include a given orbital, say ψ_{k}, that is singly occupied with spin α. The total number of such configurations is

$$M_{\mathrm{k}}^{(1)} = \binom{2g_{\mathrm{O}}-2}{n_{\mathrm{O}}-1}, \tag{9}$$

since the remaining $n_{\mathrm{O}}-1$ electrons can occupy the remaining $g_{\mathrm{O}}-1$ MOs

in all possible ways. Clearly, there is an equal number of configurations in which $\psi_{\rm k}$, is singly occupied as a β spin orbital.

Orbital $\psi_{\rm k}$ can also be doubly occupied by a spin pair. The number of such configurations, from the same arguments, is

$$M_{\rm k}^{(2)} = \binom{2g_{\rm O}-2}{n_{\rm O}-2}. \tag{10}$$

The total contribution of orbital $\psi_{\rm k}$ to a property expectation value is

$$2M_{\rm k}^{(1)} + 2M_{\rm k}^{(2)} = 2\binom{2g_{\rm O}-1}{n_{\rm O}-1}. \tag{11}$$

The average contribution of MO $\psi_{\rm k}$, allowing for the occupancies and neglecting any hyperfine interactions, is therefore the fractional occupancy

$$\nu_{\rm O} = \frac{2(M_{\rm k}^{(1)} + M_{\rm k}^{(2)})}{M^{\rm tot}} = \frac{n_{\rm O}}{g_{\rm O}}. \tag{12}$$

We note that the fractional occupancy defined in this way is such that $0 \leq \nu_{\rm O} \leq 2$, interpolates linearly between the fully occupied C shell and the empty V shell. The value $\nu_{\rm O}$ is the same for each orbital in the shell. It is clear that the value $\nu_{\rm O} = 1$ corresponds to a shell that is half occupied.

5 Configurational State Average properties

We can write molecular properties as *Aufbau* configuration state averages for n_e electrons. The π-electron density is

$$\rho_{\rm rs} = 2\sum_{\rm k\in C} {\rm U_{rk}U_{sk}^*} + \nu_{\rm O}\sum_{\rm k\in O} {\rm U_{rk}U_{sk}^*}. \tag{13}$$

The electron density matrix $\boldsymbol{\rho}$ is also known as the π charge and bond order matrix, since the atomic charge for vertex r is $q_{\rm r} = \rho_{\rm rr}$, and the π bond order for vertex pair rs is $p_{\rm rs} = \rho_{\rm rs}$ for ${\rm r} \neq {\rm s}$. Note that we can define bond order for pairs not connected by a graph edge. The bond order, $p_{\rm rs}$, measures the electron density assigned to the vertex pair rs in the electron configuration $\mathcal{C}_{\rm Auf}$, and thus for a weighted graph the π energy is related

to charges and bond orders by

$$E^{\pi} = \mathrm{Tr}(\mathbf{H}^{\pi}\boldsymbol{\rho}) = \sum_{\mathrm{r}} \alpha_{\mathrm{r}} q_{\mathrm{r}} + \sum_{\mathrm{rs}} \beta_{\mathrm{rs}} p_{\mathrm{rs}} = \beta \sum_{\mathrm{r}} E^{\pi}_{\mathrm{r}}. \tag{14}$$

Coulson and his school [10] defined the π-contribution to the bond number [5] by summing bond order contributions from the d_{r} edges incident to vertex r, which is equivalent to

$$N_{\mathrm{r}} = \sum_{\mathrm{s}\neq r} A_{\mathrm{rs}} p_{\mathrm{rs}}, \tag{15}$$

so that the contribution of atom r to total π-energy, in units of β, is

$$E^{\pi}_{\mathrm{r}} = N_{\mathrm{r}} + A_{\mathrm{rr}} q_{\mathrm{r}}. \tag{16}$$

6 Matrices of spectral moments

We now turn to more general first-order properties by introducing notation for the shell components appearing in (13) and (14), and defining *matrices of spectral moments* of the shell quantities for integral powers g:

$$t^{(g)\mathrm{C}}_{\mathrm{rs}} = \sum_{\mathrm{k}\in\mathrm{C}} \lambda^{g}_{\mathrm{k}} \mathrm{U}_{\mathrm{rk}} \mathrm{U}^{*}_{\mathrm{sk}}, \quad t^{(g)\mathrm{V}}_{\mathrm{rs}} = \sum_{\mathrm{k}\in\mathrm{V}} \lambda^{g}_{\mathrm{k}} \mathrm{U}_{\mathrm{rk}} \mathrm{U}^{*}_{\mathrm{sk}}. \tag{17}$$

In the definition for the open shell one must recognise the special case where the open shell is the nullspace (*e.g.* at $\mathcal{C}_{\mathrm{nat}}$):

$$t^{(g)\mathrm{O}}_{\mathrm{rs}} = \begin{cases} \lambda^{g}_{\mathrm{O}} \sum_{\mathrm{k}\in\mathrm{O}} \mathrm{U}_{\mathrm{rk}} \mathrm{U}^{*}_{\mathrm{sk}}, & \lambda_{\mathrm{O}} \neq 0, \\ 0, & \lambda_{\mathrm{O}} = 0. \end{cases} \tag{18}$$

These shell components satisfy normalisation conditions involving powers of the adjacency matrix:

$$t^{(g)\mathrm{C}}_{\mathrm{rs}} + t^{(g)\mathrm{O}}_{\mathrm{rs}} + t^{(g)\mathrm{V}}_{\mathrm{rs}} = (\mathbf{A}^{g})_{\mathrm{rs}}, \text{ for } g \neq 0. \tag{19}$$

Moments with *negative* g are defined by powers of the Moore-Penrose inverse $\mathbf{A}^{+}$ [1,23,24], which is constructed for both singular and non-singular

matrices from the non-zero part of the spectrum of $\mathbf{A}(G)$:

$$\mathrm{A}^{+}_{\mathrm{rs}} = \sum_{\lambda_\mathrm{k}>0} \lambda_\mathrm{k}^{-1}\mathrm{U}_{\mathrm{rk}}\mathrm{U}^{*}_{\mathrm{sk}} + \sum_{\lambda_\mathrm{k}<0} \lambda_\mathrm{k}^{-1}\mathrm{U}_{\mathrm{rk}}\mathrm{U}^{*}_{\mathrm{sk}}. \tag{20}$$

This equation makes it explicit that there is no contribution from shell K to moments with negative g. In a matrix power notation we have

$$\mathbf{A}^{g} = \begin{cases} (\mathbf{A})^{g} & \text{for } g > 0, \\ (\mathbf{A}^{+})^{|g|} & \text{for } g < 0, \\ \mathbf{A}^{0} = \mathbf{1} & \text{for } g = 0. \end{cases} \tag{21}$$

The moment of the adjacency matrix, $\mathbf{A}^{g}_{\mathrm{rs}}$, for an unweighted graph and positive integer, g, is the count of walks of length g from vertex r to s. The moments of $\mathbf{A}^{+}$ may be regarded as a generalisation to include walks of 'negative length'.

Spectral moment matrices can be used to define moments for a specific configuration, $\mathcal{C}_{\mathrm{Auf}}$, by taking weighted sums over closed and open shells

$$\mathrm{T}^{(g)}_{\mathrm{rs}} = 2t^{(g)\mathrm{C}}_{\mathrm{rs}} + \nu_\mathrm{O} t^{(g)\mathrm{O}}_{\mathrm{rs}}. \tag{22}$$

Low-order moments include the familiar properties of π-electron density (charge and bond order) $\rho_{\mathrm{rs}} = \mathrm{T}^{(0)}_{\mathrm{rs}}$, and vertex π-energy $E^{\pi}_{\mathrm{r}} = \mathrm{T}^{(1)}_{\mathrm{rr}}$.

The moments in (22) are defined in terms of our *Aufbau* configuration. We can also define corresponding *anti-Aufbau* moments in terms of those orbitals that are *empty* in $\mathcal{C}_{\mathrm{Auf}}$,

$$\overline{\mathrm{T}}^{(g)}_{\mathrm{rs}} = 2t^{(g)\mathrm{V}}_{\mathrm{rs}} + \bar{\nu}_\mathrm{O} t^{(g)\mathrm{O}}_{\mathrm{rs}}, \tag{23}$$

where $\bar{\nu}_\mathrm{O} = 2 - \nu_\mathrm{O}$ is the hole occupancy of the open shell. Assuming there are n_e electrons implied by the definitions in (22), the *anti-Aufbau* moments place $n_h = 2n - n_e$ electrons in the set of empty orbitals implied by the related *Aufbau* moment. *Aufbau* and *anti-Aufbau* moments can be considered as conjugate 'particle' and 'hole' moments, with a normalisation condition derived from (19),

$$\mathbf{T}^{(g)} + \overline{\mathbf{T}}^{(g)} = 2\mathbf{A}^{g}. \tag{24}$$

It is also convenient to introduce notation for the portion of the charge at a vertex that arises specifically from the open shell in an *Aufbau* and *anti-Aufbau* configurations:

$$q_{\mathrm{r}}^{\mathrm{O}} = \nu_{\mathrm{O}} t_{\mathrm{rr}}^{(0)\mathrm{O}}, \quad \bar{q}_{\mathrm{r}}^{\mathrm{O}} = \bar{\nu}_{\mathrm{O}} t_{\mathrm{rr}}^{(0)\mathrm{O}}. \tag{25}$$

The chemical interpretation of $q_{\mathrm{r}}^{\mathrm{O}}$ is that it is the π electronic charge density on vertex r arising from occupation of the non-bonding orbital(s), whilst the 'hole charge' $\bar{q}_{\mathrm{r}}$ is its complement.

Diagonal particle moments have special properties which make them of particular interest with regard to bounds. In particular, the even moments $\mathrm{T}_{\mathrm{rr}}^{(2g)}$ are non-decreasing as the electron count, n_e, rises from 0 to $2n$, and for each n_e they satisfy the inequality

$$0 \leq \mathrm{T}_{\mathrm{rr}}^{(2g)} \leq 2\mathbf{A}_{\mathrm{rr}}^{2g}. \tag{26}$$

For positive odd powers, the moments obey $\mathrm{T}_{\mathrm{rr}}^{(2g+1)} \geq 0$ for all electron counts and reach a maximum at or near $\mathcal{C}_{\mathrm{nat}}$ and then decrease until the value $2\mathrm{A}_{\mathrm{rr}}^{2g+1} \geq 0$ is reached by the time all levels are filled. The limiting value is zero if the graph contains no odd cycles, *i.e.* is bipartite. For negative odd powers, the limit is $(\mathbf{A}^{+})_{\mathrm{rr}}^{|2g+1|}$, which may fall below zero.

We should note a connection between the matrices of spectral moments used here and the spectral moments that have a long history in theoretical physical sciences [2–4] and graph theory [21] literatures. Spectral moments are used for example in QSAR (Quantitative Structure and Activity Relations) and QSPR (Quantitative Structure-Property Relations) [30]. In these applications the *spectral moment of order* $g > 0$ is simply

$$\mu_g = \sum_{\mathrm{k}=1}^{n} \lambda_{\mathrm{k}}^{g} = \mathrm{Tr}\mathbf{A}^{g} = \frac{1}{2}\mathrm{Tr}\left(\mathbf{T}^{(g)} + \overline{\mathbf{T}}^{(g)}\right). \tag{27}$$

For unweighted graphs, μ_g counts the total number of self-returning walks in G of length g, which encodes structural information about the graph. Burdett *et al.* [2–4] show that low-order moments μ_g can be used as a way to explain trends in stability with electron count for molecules and as a tool for diagnosing structural transitions in materials [4].

7 The ladder of moments

We defined particle and hole spectral moment matrices in (22) and (23) for *Aufbau* configurations. We now consider connections between these moments as the power g varies. We consider the quantity $(\mathbf{A}^g\boldsymbol{\rho})_{\mathrm{rs}}$ where $\boldsymbol{\rho} = \mathbf{T}^{(0)}$ is the π-electron density matrix defined in (13). Using spectral expansions we deduce that

$$\begin{aligned}(\mathbf{A}^g\boldsymbol{\rho})_{\mathrm{rs}} &= \sum_{\mathrm{k}}\sum_{\mathrm{t}} \lambda_{\mathrm{k}}^g U_{\mathrm{rk}}U_{\mathrm{tk}}^* \left(2\sum_{\ell\in\mathrm{C}} U_{\mathrm{t}\ell}U_{\mathrm{s}\ell}^* + \nu_{\mathrm{O}}\sum_{\ell\in\mathrm{O}} U_{\mathrm{t}\ell}U_{\mathrm{s}\ell}^*\right)\\ &= 2\sum_{\mathrm{k}\in\mathrm{C}} \lambda_{\mathrm{k}}^g U_{\mathrm{rk}}U_{\mathrm{sk}}^* + \nu_{\mathrm{O}}\sum_{\mathrm{k}\in\mathrm{O}} \lambda_{\mathrm{k}}^g U_{\mathrm{rk}}U_{\mathrm{sk}}^* = \mathrm{T}_{\mathrm{rs}}^{(g)},\end{aligned} \tag{28}$$

where we used the orthonormality of the MOs for the sum over index t. In the same manner, it can be shown that

$$(\mathbf{A}^g\bar{\boldsymbol{\rho}})_{\mathrm{rs}} = \overline{\mathrm{T}}_{\mathrm{rs}}^{(g)}, \tag{29}$$

where the hole density is

$$\bar{\boldsymbol{\rho}} = 2.\mathbf{1} - \boldsymbol{\rho}. \tag{30}$$

These relations for chains of particle and hole spectral moments also apply for positive and negative integral values of g, provided we interpret the negative powers using the Moore-Penrose inverse, as indicated in (20) and (21). All moment matrices can be calculated from zeroth order moments (charges and bond orders) and the generalised walk matrices $\mathbf{A}^g$.

The ladder of relationships can be made explicit using matrix notation:

$$\mathbf{T}^{(g)} = \mathbf{A}\mathbf{T}^{(g-1)} \text{ and } \overline{\mathbf{T}}^{(g)} = \mathbf{A}\overline{\mathbf{T}}^{(g-1)}. \tag{31}$$

The Moore-Penrose inverse acts as a lowering operator, so

$$\mathbf{T}^{(g)} = \mathbf{A}^+\mathbf{T}^{(g+1)}, \text{ and } \overline{\mathbf{T}}^{(g)} = \mathbf{A}^+\overline{\mathbf{T}}^{(g+1)}. \tag{32}$$

This property follows from the fact that $\mathbf{A}\mathbf{A}^+$ is a projection operator

$$\mathbf{A}\mathbf{A}^+ = \mathbf{1} - \mathbf{P}^{\mathrm{K}}, \tag{33}$$

where

$$\mathbf{P}^{\mathrm{K}}_{\mathrm{rs}} = \sum_{\mathrm{k}\in\mathrm{K}} \mathrm{U}_{\mathrm{rk}}\mathrm{U}^{*}_{\mathrm{sk}}, \tag{34}$$

is a projector ($(\mathbf{P}^{\mathrm{K}})^2 = \mathbf{P}^{\mathrm{K}}$) onto the nullspace. Matrix $\mathbf{T}^{(g)}$ and its hole counterpart have no nullspace component (*i.e.* $\mathbf{P}^{\mathrm{K}}\mathbf{T}^{(g)} = \mathbf{0}$) when $g \neq 0$. The relationships (28)-(32) apply to any *Aufbau* configuration, and make clear the separate roles of the graphical information contained in $\mathbf{A}^g$, and the electronic information contained in the electron density, $\boldsymbol{\rho}$. This distinction emerges sharply when we restrict our considerations to the *natural* configuration, $\mathcal{C}_{\mathrm{nat}}$ of *bipartite* graphs.

8 Spectral moments for bipartite graphs

Bipartite graphs contain two disjoint sets of vertices, $\{V_1\}$ and $\{V_2\}$, with sizes $n_1 = |V_1|$ and $n_2 = |V_2|$, such that the two ends of every edge lie in different sets. The adjacency matrix can then be blocked as

$$\mathbf{A} = \begin{pmatrix} \mathbf{0} & \mathbf{B} \\ \mathbf{B}^{\mathrm{T}} & \mathbf{0} \end{pmatrix}, \tag{35}$$

where vertices are ordered by set, $\{V_1\}$ then $\{V_2\}$. Hence, even moments of the adjacency matrix connect vertices in the same partite set, whilst odd moments connect vertices in different partite sets, as shown below:

$$\mathbf{A}^{2g} = \begin{pmatrix} (\mathbf{B}\mathbf{B}^{\mathrm{T}})^g & \mathbf{0} \\ \mathbf{0} & (\mathbf{B}^{\mathrm{T}}\mathbf{B})^g \end{pmatrix}, \mathbf{A}^{2g+1} = \begin{pmatrix} \mathbf{0} & \mathbf{B}(\mathbf{B}^{\mathrm{T}}\mathbf{B})^g \\ \mathbf{B}^{\mathrm{T}}(\mathbf{B}\mathbf{B}^{\mathrm{T}})^g & \mathbf{0} \end{pmatrix}. \tag{36}$$

Powers of the Moore-Penrose inverse, $\mathbf{A}^{+}$, have an analogous alternating block structure. In particular, $\mathrm{A}^{+}_{\mathrm{rs}}$ vanishes for r and s in the same set. The π-density matrix, $\widetilde{\boldsymbol{\rho}}$, at $\mathcal{C}_{\mathrm{nat}}$ for a bipartite graph also has a block structure:

$$\widetilde{\boldsymbol{\rho}} = \begin{pmatrix} \mathbf{1} & \widetilde{\boldsymbol{\rho}}_{12} \\ \widetilde{\boldsymbol{\rho}}^{\mathrm{T}}_{12} & \mathbf{1} \end{pmatrix}, \tag{37}$$

which is a consequence of the pairing theorem. The argument is as follows: (13) shows contributions from shell C (the space of the positive eigenvalues

for $\mathcal{C}_{\rm nat}$) and from the open shell O (the nullspace for $\mathcal{C}_{\rm nat}$ and with $\nu_{\rm O} = 1$). From the theorem, positive and negative eigenvalues are paired such that form every $\lambda_{\rm k} > 0$, there is a $\lambda_{\bar{\rm k}} = -\lambda_{\rm k}$ and corresponding eigenvectors have $\mathrm{U}_{\rm rk} = \mathrm{U}_{\rm r\bar{k}}$ for one partite set, and $\mathrm{U}_{\rm rk} = -\mathrm{U}_{\rm r\bar{k}}$ for the other. This immediately gives $t_{\rm rs}^{(0)\rm C} = t_{\rm rs}^{(0)\rm V}$ when r and s are in the same partite set, and it is easily shown, using orthonormality, that the matrix elements in the diagonal blocks of $\boldsymbol{\rho}$ are delta functions. The chemical corollary is the sometimes forgotten fact that the Coulson bond order vanishes for all pairs of vertices in the same partite set.

As the graph is bipartite, the off-diagonal blocks have no nullspace contributions since every nullspace eigenvector can be restricted to non-zero entries from just one or other of the partite sets. The off-diagonal block contributions can therefore be calculated from

$$(\widetilde{\rho}_{12})_{\rm rs} = 2\sum_{\rm k\in C} \mathrm{U}_{\rm rk}\mathrm{U}^{*}_{\rm sk}. \tag{38}$$

All non-zero moments can now be deduced from (36) and (37) as

$$\widetilde{\mathbf{T}}^{(2g)} = \begin{pmatrix} (\mathbf{B}^{\rm T}\mathbf{B})^{g} & (\mathbf{B}^{\rm T}\mathbf{B})^{g}\widetilde{\boldsymbol{\rho}}_{12} \\ (\mathbf{B}\mathbf{B}^{\rm T})^{g}\widetilde{\boldsymbol{\rho}}_{12}^{\rm T} & (\mathbf{B}\mathbf{B}^{\rm T})^{g} \end{pmatrix} = \mathbf{A}^{2g} + \begin{pmatrix} \mathbf{0} & (\mathbf{B}^{\rm T}\mathbf{B})^{g}\widetilde{\boldsymbol{\rho}}_{12} \\ (\mathbf{B}\mathbf{B}^{\rm T})^{g}\widetilde{\boldsymbol{\rho}}_{12}^{\rm T} & \mathbf{0} \end{pmatrix}. \tag{39}$$

The diagonal blocks of the even spectral moments for the natural configurations of bipartite graphs are the generalised walk matrices. They are purely graph theoretical quantities. The equivalent expression for odd moments is

$$\widetilde{\mathbf{T}}^{(2g+1)} = \begin{pmatrix} (\mathbf{B}\mathbf{B}^{\rm T})^{g}\mathbf{B}\widetilde{\boldsymbol{\rho}}_{12}^{\rm T} & \mathbf{0} \\ \mathbf{0} & (\mathbf{B}^{\rm T}\mathbf{B})^{g}\mathrm{B}^{\rm T}\widetilde{\boldsymbol{\rho}}_{12} \end{pmatrix}. \tag{40}$$

9 Property profiles

It may be useful at this point to discuss qualitative differences amongst first-order properties defined in terms of configuration state averages. All are invariant to unitary transformations amongst orbitals within each degenerate shell (eigenspace). This is ensured by the configuration state average formulation and the introduction of fractional occupation. However,

when we look at the variation of properties with electron count, differences emerge. For all of the properties, the values at zero occupation are known. For particle properties $\mathrm{T}_{\mathrm{rs}}^{(g)}$ (including charge, energy, bond order and bond number) the limits are 0 for the empty π-system and $2\mathbf{A}_{\mathrm{rs}}^{g}$ at full occupation of the π/π^* manifold. Hole properties take complementary values since $\overline{\mathrm{T}}_{\mathrm{rs}}^{(g)} = 2\mathbf{A}_{\mathrm{rs}}^{g} - \mathrm{T}_{\mathrm{rs}}^{(g)}$. By the nature of a configuration state average, the properties vary linearly with electron number as a shell is being filled, *i.e.* as ν_{O} advances in steps of 1 from 0 to $2g_{\mathrm{O}}$. The slope of this line may be zero in two circumstances; when vertex r or s is λ_{k}-CFV, or for a spectral moment with $g \neq 0$ when the open shell is non-bonding ($\lambda_{\mathrm{O}} = 0$). The one shell guaranteed to have positive slope for $\mathrm{T}_{\mathrm{rs}}^{(g)}$ is the non-degenerate LOMO, corresponding to the Perron eigenvalue λ_1, which has a full vector of positive entries. Hence the profile of a particle property at general electron counts follows one of several generic patterns. Some properties have a 'ziggurat' profile, *i.e.* ascending from zero, possibly *via* regions of zero gradient, reaching their highest value at or before $\mathcal{C}_{\mathrm{nat}}$, and descending towards the final value with non-positive slope. Examples of ziggurat properties are the diagonal matrix elements of odd spectral moments. Other properties have a 'stepped ramp' profile from zero to $2n$ electrons; examples are the diagonal matrix elements of the even spectral moments. A profile of the third kind rises initially from 0 and reaches the end point from either above or below the axis.

Chemical information is encoded in the profiles. The conceptual advantage of the bond number, related to its ziggurat profile, is that it characterises non-bonding shells. In this picture, a non-bonding shell is precisely one where all bond numbers N_{r}, are independent of occupation, ν_{O}. In

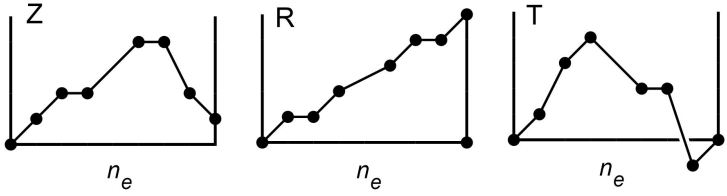

Figure 1. Generic property profiles for spectral moments of ziggurat (**Z**), ramp (**R**), or third kind (**T**), as functions of n_e.

contrast, individual bond orders, $p_{\rm rs}$, which follow a profile the third kind, may have bonding, non-bonding, or anti-bonding variation with $\nu_{\rm O}$ as long as the changes in all bonds incident on a given centre cancel. Similarly, the Hückel energy has a ziggurat profile since all bond numbers have a profile of this kind. The top of the ziggurat is the maximum achievable π-energy for the system, equal to the graph energy, E^G, and hence (in units of β),

$$\widetilde{E}^{\pi} = 2 \sum_{\lambda_{\rm k}>0} \lambda_{\rm k} = \sum_{\rm k} |\lambda_{\rm k}| = E^G, \tag{41}$$

which reveals the precise nature of the relationship between the mathematical and chemical quantities, answering Estrada's rhetorical question [15].

10 Bounds to spectral moments

In this section we derive bounds of two kinds. The first, *configurational bounds*, are functions of electron number. The second, *non-configurational bounds*, are independent of electron number and depend only on the underlying graph, G. In the following discussion, we shall add a notational convention, namely that properties evaluated at $\mathcal{C}_{\rm nat}$ will be signified by adding a tilde. Hence $\tilde{q}_{\rm r}, \tilde{N}_{\rm r}, \widetilde{\rm T}_{\rm rs}^{(g)}$, *etc.* will signify charge, bond number and spectral moment matrix elements for $\mathcal{C}_{\rm nat}$.

There is a subtlety in the definition of configurational and non- configurational bounds in that some bounds may be valid for only part of the full range of particle or hole counts, as they have been defined in terms of a functional that is well behaved for only part of the range. A typical pattern is that of the *partial bound* which is valid for particle (electron) numbers in the range $0 \leq n_e \leq 2n_+ + 2\eta$, where n_+ is the number of MOs with positive eigenvalues, and η is the nullspace degeneracy. The same phenomenon can occur for hole moments with the number of holes in the range $0 \leq n_h \leq 2n_- + 2\eta$, where n_- is the number of MOs with negative eigenvalues, and $n_h = 2n - n_e$. Left and right bounds coincide at $\mathcal{C}_{\rm nat}$, or indeed for any configuration with partial occupation of the nullspace.

10.1 The Gutman bounds

Gutman [18] considered bounds for a number of molecular properties, including the bond number, localisation energy and atom-atom polarisability. He derived two theorems for bipartite graphs with even numbers of vertices. The first theorem (GT) states bounds for the bond number which in our notation are

$$\text{(GT)} \qquad \lambda_+ \leq \tilde{N}_\mathrm{r} \leq \lambda_1, \tag{42}$$

where λ_1 and λ_+ are the largest and smallest positive eigenvalues of the adjacency matrix. In fact, the proof given in [18] applies strictly to CFV in bipartite graphs, as discussed in the section below.

The second theorem (GT′) was derived for trees,

$$\text{(GT}') \qquad \tilde{N}_\mathrm{r} \leq a_\mathrm{r} = \sqrt{d_\mathrm{r}}, \tag{43}$$

and corresponds to a subcase of what we have called the Coulson-Moffitt bound; the general case for unweighted graphs was finally proved only recently with a different method [17].

10.1.1 Analysis of the proof of GT

The starting point of the proof of GT in [18] is an old expression from Coulson's work for bond number [9], where an integral over the 'Coulson contour' is replaced by a line integral with real integrand

$$\widetilde{N}_\mathrm{r} = \int_{-\infty}^{\infty} (1 - xV)dx, \tag{44}$$

where $V(x)$ is the Green's function

$$V(x) = i\frac{P_{G-\mathrm{r}}(ix)}{P(ix)}, \tag{45}$$

and $P(E)$ and $P_{G-\mathrm{r}}(E)$ are the characteristic polynomials for the graph G and the vertex deleted graph $G-\mathrm{r}$. Interlacing gives the relationship between the roots μ of $P_{G-\mathrm{r}}(E)$ and the roots λ of $P(E)$, and the pairing theorem allows $V(x)$ to be expressed explicitly. We distinguish the two cases where vertex r is a CV or a CFV of a bipartite graph with nullity η.

For a CFV (necessarily an upper CFV for a bipartite graph) we have

$$V(x) = \frac{x}{x^2+\lambda_+^2} \prod_{i=1}^{n_+-1} \left(\frac{x^2+\mu_i^2}{x^2+\lambda_i^2} \right). \tag{46}$$

Interlacing, $\lambda_i \leq \mu_i \leq \lambda_{i+1}$, now allows replacement of the non-trivial factors by upper and lower bounds

$$\frac{x}{x^2+\lambda_1^2} \leq V(x) \leq \frac{x}{x^2+\lambda_+^2}, \tag{47}$$

to give (42) for a CFV.

For a CV we have a different expression for $V(x)$:

$$V(x) = \frac{1}{x} \prod_{i=1}^{n_+} \left(\frac{x^2+\mu_i^2}{x^2+\lambda_i^2} \right), \tag{48}$$

and the same technique leads to a zero integrand, and hence

$$0 \leq \widetilde{N}_\mathrm{r} \leq \lambda_1. \tag{49}$$

Hence, strictly, GT as proved applies to CFV in bipartite graphs, with a weaker lower bound for CV, where trivially $N_\mathrm{r}{>}0$. It is possible to derive more accurate bounds using this methodology to take extra eigenvalues into account. Given the reliance on the pairing theorem, the derivation outlined above does not easily extend to non-bipartite graphs.

10.1.2 Gutman-style bounds for particle spectral moments

Results like GT can be derived for any spectral moment that involves a non-zero power of the eigenvalue. We now prove an extended form of Gutman bound for all electron counts and graphs, by applying the spectral moments defined in (22) as

$$\mathrm{T}_{\mathrm{rr}}^{(g)} = 2\sum_{\mathrm{k}\in\mathrm{C}} \lambda_\mathrm{k}^g |\mathrm{U}_{\mathrm{rk}}|^2 + \lambda_\mathrm{O}^g q_\mathrm{r}^\mathrm{O}. \tag{50}$$

The relevant case is $g{\neq}0$. These bounds will be referred to as Gutman type bounds as they depend on powers of large and small eigenvalues, although they also involve charges, and it is this second feature that is crucial to their applicability to all graphs and vertices. To find bounds for $\mathrm{T}_{\mathrm{rr}}^{(g)}$, we

note that if the configuration, $\mathcal{C}_{\mathrm{Auf}}$ has only positive eigenvalues in the C shell, and $\lambda_{\mathrm{O}}{\geq}0$, no terms in (50) are negative. In this case, we can achieve upper and lower bound formulae by replacing λ_{k} by either λ_1 or λ_+:

$$\begin{aligned} 2\lambda_+^g t_{\mathrm{rr}}^{(0)\mathrm{C}} + \lambda_{\mathrm{O}}^g q_{\mathrm{r}}^{\mathrm{O}} \leq \mathrm{T}_{\mathrm{rr}}^{(g)} \leq 2\lambda_1^g t_{\mathrm{rr}}^{(0)\mathrm{C}} + \lambda_{\mathrm{O}}^g q_{\mathrm{r}}^{\mathrm{O}}, \qquad & g > 0, \\ 2\lambda_1^g t_{\mathrm{rr}}^{(0)\mathrm{C}} + \lambda_{\mathrm{O}}^g q_{\mathrm{r}}^{\mathrm{O}} \leq \mathrm{T}_{\mathrm{rr}}^{(g)} \leq 2\lambda_+^g t_{\mathrm{rr}}^{(0)\mathrm{C}} + \lambda_{\mathrm{O}}^g q_{\mathrm{r}}^{\mathrm{O}}, \qquad & g < 0. \end{aligned} \tag{51}$$

In (51) the bounds involving λ_1 are valid for the whole range of electron count, but those involving λ_+ apply only within the range $0{\leq}n_e{\leq}2n_+ + 2n_{\mathrm{O}}$. The highest electron count for which both bounds apply therefore corresponds to full occupation of all positive eigenvalue states and the nullspace (if any). The range includes $\mathcal{C}_{\mathrm{nat}}$. We can eliminate $t_{\mathrm{rr}}^{(0)\mathrm{C}}$ for $g{\neq}0$ in (51) by using the fact that

$$2t_{\mathrm{rr}}^{(0)\mathrm{C}} = \left(q_{\mathrm{r}} - q_{\mathrm{r}}^{\mathrm{O}}\right), \tag{52}$$

to give bounds in terms of eigenvalues and total and open-shell π-charges:

$$\begin{aligned} \lambda_+^g q_{\mathrm{r}} + (\lambda_{\mathrm{O}}^g - \lambda_+^g) q_{\mathrm{r}}^{\mathrm{O}} \leq \mathrm{T}_{\mathrm{rr}}^{(g)} \leq \lambda_1^g q_{\mathrm{r}} + (\lambda_{\mathrm{O}}^g - \lambda_1^g) q_{\mathrm{r}}^{\mathrm{O}}, \qquad & g > 0, \\ \lambda_1^g q_{\mathrm{r}} + (\lambda_{\mathrm{O}}^g - \lambda_1^g) q_{\mathrm{r}}^{\mathrm{O}} \leq \mathrm{T}_{\mathrm{rr}}^{(g)} \leq \lambda_+^g q_{\mathrm{r}} + (\lambda_{\mathrm{O}}^g - \lambda_+^g) q_{\mathrm{r}}^{\mathrm{O}}, \qquad & g < 0. \end{aligned} \tag{53}$$

This is the appropriate generalisation of GT for the spectral moments with $g{\neq}0$, for all graphs and vertex types. Note that in the expressions (53) the contribution of shell O is accounted for exactly by the introduction of $q_{\mathrm{r}}^{\mathrm{O}}$. Hence we refer to this style of bound as GSOp (Gutman-style open-shell particle bound). The GSOp bound involving λ_1 is exact for all graphs where the eigenspace corresponding to λ_2 is less than full. Of course, if the graph has only a single positive eigenvalue and no antibonding electrons are present, GSOp upper and lower bounds are both exact.

Note that in deriving (53) we made a specific choice about the role of the open shell eigenvalue λ_{O}, i.e. using its exact value whenever the configuration is open shell, but replacing it by the bounding eigenvalue (λ_1 or λ_+, respectively) when that shell becomes full. This leads to a jump in value when $\nu_{\mathrm{O}}{=}2$. Another choice would have been to replace *all* eigenvalues in the spectral moment expression by the bounding eigenvalue: this has the advantage of simplicity but leads to larger errors over the range

of electron numbers. Equation (53) would then become

$$\begin{aligned} \lambda_+^g q'_{\rm r} \le {\rm T}_{\rm rr}^{(g)} \le \lambda_1^g q'_{\rm r}, \qquad & g>0, \\ \lambda_1^g q'_{\rm r} \le {\rm T}_{\rm rr}^{(g)} \le \lambda_+^g q'_{\rm r}, \qquad & g<0. \end{aligned} \tag{54}$$

where we have used $q'_{\rm r} = q_{\rm r} - q_{\rm r}^{\rm K}$ as a shorthand for the charge at vertex r corrected for any charge present in the kernel (non-bonding) eigenspace. We refer to this alternative choice as GSp (Gutman-style particle bound). The GSp bound is exact for $n_e \le 2$, and also for all graphs with a single positive eigenvalue when no antibonding orbitals are occupied.

10.1.3 Gutman-style bounds for hole spectral moments

We can also use this approach to derive a bound analogous to (53) for the *hole* spectral moment, $\overline{\rm T}_{\rm rr}^{(g)}$, by using (23) and (25) to write

$$\overline{\rm T}_{\rm rr}^{(g)} = 2\sum_{\rm k\in V} \lambda_{\rm k}^g |{\rm U}_{\rm rk}|^2 + \lambda_{\rm O}^g \bar{q}_{\rm r}^{\rm O}. \tag{55}$$

Provided we do not allow positive $\lambda_{\rm k}$ to appear in the formulae we can adapt the methodology for particle spectral moments, using the *largest* and *smallest* negative eigenvalues λ_- and λ_- to derive the analogue of (51):

$$\begin{aligned} 2\lambda_n^g t_{\rm rr}^{(0){\rm V}} + \lambda_{\rm O}^g \bar{q}_{\rm r}^{\rm O} \ge 2\mathbf{A}_{\rm rr}^g - {\rm T}_{\rm rr}^{(g)} \ge 2\lambda_-^g t_{\rm rr}^{(0){\rm V}} + \lambda_{\rm O}^g \bar{q}_{\rm r}^{\rm O}, \qquad & g>0, \text{ even} \\ 2\lambda_-^g t_{\rm rr}^{(0){\rm V}} + \lambda_{\rm O}^g \bar{q}_{\rm r}^{\rm O} \ge 2\mathbf{A}_{\rm rr}^g - {\rm T}_{\rm rr}^{(g)} \ge 2\lambda_n^g t_{\rm rr}^{(0){\rm V}} + \lambda_{\rm O}^g \bar{q}_{\rm r}^{\rm O}, \qquad & g>0, \text{ odd}\,. \end{aligned} \tag{56}$$

The inequalities in (56) flip over when $g<0$. Using

$$2t_{\rm rr}^{(0){\rm V}} = \left(\bar{q}_{\rm r} - \bar{q}_{\rm r}^{\rm O}\right), \tag{57}$$

we again obtain partial bounds on terms of $q_{\rm r}$, $q_{\rm r}^{\rm O}$, λ_n, λ_-, and $\lambda_{\rm O}$:

$$\begin{aligned} \lambda_n^g \left(\bar{q}_{\rm r} - \bar{q}_{\rm r}^{\rm O}\right) + \lambda_{\rm O}^g \bar{q}_{\rm r}^{\rm O} \ge 2\mathbf{A}_{\rm rr}^g - {\rm T}_{\rm rr}^{(g)} \ge \lambda_-^g \left(\bar{q}_{\rm r} - \bar{q}_{\rm r}^{\rm O}\right) + \lambda_{\rm O}^g \bar{q}_{\rm r}^{\rm O}, \qquad & g>0, \text{ even} \\ \lambda_-^g \left(\bar{q}_{\rm r} - \bar{q}_{\rm r}^{\rm O}\right) + \lambda_{\rm O}^g \bar{q}_{\rm r}^{\rm O} \ge 2\mathbf{A}_{\rm rr}^g - {\rm T}_{\rm rr}^{(g)} \ge \lambda_n^g \left(\bar{q}_{\rm r} - \bar{q}_{\rm r}^{\rm O}\right) + \lambda_{\rm O}^g \bar{q}_{\rm r}^{\rm O}, \qquad & g>0, \text{ odd}\,. \end{aligned} \tag{58}$$

By analogy to GSOp, we refer to this bound as GSOh. If we replace $\lambda_{\rm O}$ by the bounding eigenvalues λ_n or λ_- we obtain GSh. Special cases where one or both bounds of GSOh or GSh are exact can be inferred.

Figure 2 shows the particle and hole bounds as a function of electron number in the example of C_{60}. The jump in values for GSO as an open shell closes (ν_O=2) is apparent in the left hand panel. The GSO bound has lower errors over most of the range, but GS and GSO values at $\mathcal{C}_{\rm nat}$ are equal.

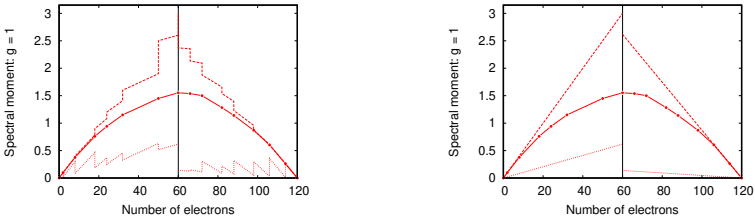

Figure 2. C_{60} bond numbers (solid) with points at shell boundaries. Particle and hole GSO bounds in the left panel and GS bounds in the right (dashed - upper bound, dotted -lower bound). $\mathcal{C}_{\rm nat}$ has n_e=60. Particle bounds to the left of $\mathcal{C}_{\rm nat}$ and hole bounds to the right.

10.1.4 Property bounds at the natural configuration

Further simplifications can be made using the ideas of core and core-forbidden vertices. At $\mathcal{C}_{\rm nat}$, either there is no open shell O = K, as G is non-singular, and hence $\widetilde{q}_{\rm r}^{\rm O} = 0$ for all r, or there is an open shell with $\lambda_{\rm K} = 0$ and $\widetilde{q}_{\rm r}^{\rm K} = 0$ for all CFV but $\widetilde{q}_{\rm r}^{\rm K} > 0$ for CV.

The various combinations of configuration, vertex and graph type are listed below, using labelling (X:Y:Z) where X is the configuration, Y is the vertex type and Z is the graph type ('bip' for bipartite, 'all' for general graphs). We use the fact that $\tilde{q}_{\rm r}$=1 for all vertices in a bipartite graph. For a bipartite molecular graph, $0<q_{\rm r}^{\rm O}\leq 1$. In the natural configuration (53) and (54) are equivalent. The cases are:

($\mathcal{C}_{\rm nat}$: CV: all)
$$\begin{aligned} &\lambda_+^g(\tilde{q}_{\rm r}-\tilde{q}_{\rm r}^{\rm K}) \leq \widetilde{\rm T}_{\rm rr}^{(g)} \leq \lambda_1^g(\tilde{q}_{\rm r}-\tilde{q}_{\rm r}^{\rm K}), && g>0,\\ &\lambda_1^g(\tilde{q}_{\rm r}-\tilde{q}_{\rm r}^{\rm K}) \leq \widetilde{\rm T}_{\rm rr}^{(g)} \leq \lambda_+^g(\tilde{q}_{\rm r}-\tilde{q}_{\rm r}^{\rm K}), && g<0. \end{aligned} \tag{59}$$

($\mathcal{C}_{\rm nat}$: CFV: all)
$$\begin{aligned} &\lambda_+^g\tilde{q}_{\rm r} \leq \widetilde{\rm T}_{\rm rr}^{(g)} \leq \lambda_1^g\tilde{q}_{\rm r}, && g>0,\\ &\lambda_1^g\tilde{q}_{\rm r} \leq \widetilde{\rm T}_{\rm rr}^{(g)} \leq \lambda_+^g\tilde{q}_{\rm r}, && g<0. \end{aligned} \tag{60}$$

($\mathcal{C}_{\rm nat}$: CV: bip)
$$\lambda_+^g(1-\widetilde{q}_{\rm r}^{\rm K}) \le \widetilde{\rm T}_{\rm rr}^{(g)} \le \lambda_1^g(1-\widetilde{q}_{\rm r}^{\rm K}) \qquad g>0,$$
$$\lambda_1^g(1-\widetilde{q}_{\rm r}^{\rm K}) \le \widetilde{\rm T}_{\rm rr}^{(g)} \le \lambda_+^g(1-\widetilde{q}_{\rm r}^{\rm K}), \qquad g<0. \tag{61}$$

($\mathcal{C}_{\rm nat}$: CFV: bip)
$$\lambda_+^g \le \widetilde{\rm T}_{\rm rr}^{(g)} \le \lambda_1^g, \qquad g>0,$$
$$\lambda_1^g \le \widetilde{\rm T}_{\rm rr}^{(g)} \le \lambda_+^g, \qquad g<0. \tag{62}$$

Note that for CV in bipartite graphs at $\mathcal{C}_{\rm nat}$, the term $1-\widetilde{q}_{\rm r}^{\rm K}$ in (61) implies $\widetilde{\rm T}_{\rm rr}^{(g)} < \lambda_1^g$.

10.2 Cauchy-Schwarz configurational bounds

We can derive further property bounds that depend on electron number using the well known Cauchy-Schwarz (CS) inequality. The CS inequality [6, 29] relates the scalar product of two m-dimensional vectors $|a\rangle = (a_1, a_2, \cdots, a_m)$ and $|b\rangle = (b_1, b_2, \cdots, b_m)$ to the squared norms

$$|\,\langle a \mid b\rangle\,|^2 \;\le\; \langle a \mid a\rangle\,\langle b \mid b\rangle\,, \tag{63}$$

where

$$\langle a \mid b\rangle = \sum_{\rm k} a_{\rm k}^* b_{\rm k}. \tag{64}$$

For our purpose, we define a set of vectors indexed by state labels, k, and limited to the fully and partially occupied MOs that define a particular *Aufbau* configuration with a closed shell C and an open shell O:

$$x(\mathrm{r},g)_{\rm k} = \begin{cases} \sqrt{2}\lambda_{\rm k}^g U_{\rm rk}, & {\rm k} \in {\rm C}\backslash{\rm K} \\ \sqrt{\nu_{\rm O}}\lambda_{\rm O}^g U_{\rm rk}, & {\rm k} \in {\rm O}\backslash{\rm K}. \end{cases} \tag{65}$$

In this form the vector is appropriate for defining expressions for *particle* moments. Note that this expression for x excludes terms involving kernel vectors. The discussion is initially for spectral moments where g is a nonzero integer, and such moments do not contain *any* contributions from the nullspace shell, K, whether g be positive or negative. Therefore, for consistency, we have limited the entries in the x vector to ${\rm k} \notin {\rm K}$ in our *Aufbau* configuration. We note for later that $g = 0$ spectral moments

(charges and bond orders) contain nullspace contributions. From (65)

$$\langle \boldsymbol{x}(\mathrm{r},g) \mid \boldsymbol{x}(\mathrm{s},g)\rangle = \mathrm{T}_{\mathrm{rs}}^{(2g)\prime}, \tag{66}$$

where $\mathrm{T}_{\mathrm{rr}}^{(g)\prime} = \mathrm{T}_{\mathrm{rr}}^{(g)}$, $\forall g \neq 0$, but

$$\mathrm{T}_{\mathrm{rs}}^{(0)\prime} = \begin{cases} \mathrm{T}_{\mathrm{rs}}^{(0)}, & 0 \leq n_e \leq 2n_+, \\ \mathrm{T}_{\mathrm{rs}}^{(0)} - \nu_{\mathrm{K}} \sum_{\mathrm{k}\in\mathrm{K}} \mathrm{U}_{\mathrm{rk}}\mathrm{U}_{\mathrm{sk}}^{*}, & 2n_+ < n_e \leq 2n_+ + 2\eta, \\ \mathrm{T}_{\mathrm{rs}}^{(0)} - 2\sum_{\mathrm{k}\in\mathrm{K}} \mathrm{U}_{\mathrm{rk}}\mathrm{U}_{\mathrm{sk}}^{*}, & 2n_+ + 2\eta < n_e \leq 2n. \end{cases} \tag{67}$$

In this notation the CS inequality (63) is

$$\mid \mathrm{T}_{\mathrm{rs}}^{(h+g)\prime} \mid^2 = \mid \langle \boldsymbol{x}(\mathrm{s},h) \mid \boldsymbol{x}(\mathrm{r},g)\rangle \mid^2 \leq \mathrm{T}_{\mathrm{rr}}^{(2g)\prime}\mathrm{T}_{\mathrm{ss}}^{(2h)\prime}. \tag{68}$$

As the eigenvalue factors in (65) are multiplicative, it is possible to associate the eigenvalue powers g or h with either x factor, and conclude that e.g.,

$$\mid \mathrm{T}_{\mathrm{rs}}^{(h+g)\prime} \mid^2 = \mid \langle \boldsymbol{x}(\mathrm{r},h) \mid \boldsymbol{x}(\mathrm{s},g)\rangle \mid^2 \leq \mathrm{T}_{\mathrm{ss}}^{(2g)\prime}\mathrm{T}_{\mathrm{rr}}^{(2h)\prime}. \tag{69}$$

We can also develop bounds for the hole spectral moments by defining

$$\bar{x}(\mathrm{r},g)_{\mathrm{k}} = \begin{cases} \sqrt{2}\lambda_{\mathrm{k}}^{g} U_{\mathrm{rk}}, & \mathrm{k} \in \mathrm{V}\backslash\mathrm{K} \\ \sqrt{\bar{\nu}_{\mathrm{O}}}\lambda_{\mathrm{O}}^{g} U_{\mathrm{rk}}, & \mathrm{k} \in \mathrm{O}\backslash\mathrm{K}, \end{cases} \tag{70}$$

which leads to the equation analogous to (68),

$$\mid \overline{\mathrm{T}}_{\mathrm{rs}}^{(h+g)\prime} \mid^2 = \mid \langle \bar{\boldsymbol{x}}(\mathrm{s},h) \mid \bar{\boldsymbol{x}}(\mathrm{r},g)\rangle \mid^2 \leq \overline{\mathrm{T}}_{\mathrm{rr}}^{(2g)\prime}\overline{\mathrm{T}}_{\mathrm{ss}}^{(2h)\prime}, \tag{71}$$

where $\overline{\mathrm{T}}_{\mathrm{rr}}^{(g)\prime} = \overline{\mathrm{T}}_{\mathrm{rr}}^{(g)}$, $\forall g \neq 0$, but

$$\overline{\mathrm{T}}_{\mathrm{rs}}^{(0)\prime} = \begin{cases} \overline{\mathrm{T}}_{\mathrm{rs}}^{(0)} - 2\sum_{\mathrm{k}\in\mathrm{K}} \mathrm{U}_{\mathrm{rk}}\mathrm{U}_{\mathrm{sk}}^{*}, & 2n_- + 2\eta < n_h \leq 2n, \\ \overline{\mathrm{T}}_{\mathrm{rs}}^{(0)} - \bar{\nu}_{\mathrm{K}} \sum_{\mathrm{k}\in\mathrm{K}} \mathrm{U}_{\mathrm{rk}}\mathrm{U}_{\mathrm{sk}}^{*}, & 2n_- < n_h \leq 2n_- + 2\eta, \\ \overline{\mathrm{T}}_{\mathrm{rs}}^{(0)}, & 0 \leq n_h \leq 2n_-. \end{cases} \tag{72}$$

The three ranges of hole occupancy correspond respectively to the electron occupancies in the three lines of (67), since $n_h = 2n - n_e$.

10.2.1 CS bounds for odd spectral moments

Bounds for odd spectral moments are generated by putting $h = g{+}1$ in (68) and (71) to give bounds for the unprimed moments, since $\mathrm{T}_{\mathrm{rr}}^{(2g+1)\prime} = \mathrm{T}_{\mathrm{rr}}^{(2g+1)}$:

$$| \mathrm{T}_{\mathrm{rs}}^{(2g+1)} |^2 \leq \mathrm{T}_{\mathrm{rr}}^{(2g)\prime} \mathrm{T}_{\mathrm{ss}}^{(2g+2)\prime}, \quad | \overline{\mathrm{T}}_{\mathrm{rs}}^{(2g+1)} |^2 \leq \overline{\mathrm{T}}_{\mathrm{rr}}^{(2g)\prime} \overline{\mathrm{T}}_{\mathrm{ss}}^{(2g+2)\prime}. \tag{73}$$

This expresses odd moments in terms of even moments that step up and down by one in the power. In the specific case of bond number, CS particle and hole bounds (73) become, assuming $\mathrm{A}_{\mathrm{rr}} = 0$,

$$(N_{\mathrm{r}})^2 \leq q_{\mathrm{r}}' \mathrm{T}_{\mathrm{rr}}^{(2)}, \qquad (\overline{N}_{\mathrm{r}})^2 = (N_{\mathrm{r}})^2 \leq \bar{q}_{\mathrm{r}}' \overline{\mathrm{T}}_{\mathrm{rr}}^{(2)}. \tag{74}$$

The adjacency matrix for undirected graphs is hermitian, and we can always choose the eigenvector entries, and hence the vector coefficients in (65), (70), to be real. In such a case we may take square roots, to give

$$\begin{aligned} -\sqrt{\mathrm{T}_{\mathrm{rr}}^{(2g)\prime} \mathrm{T}_{\mathrm{ss}}^{(2g+2)\prime}} \leq \quad & \mathrm{T}_{\mathrm{rs}}^{(2g+1)} \quad \leq \sqrt{\mathrm{T}_{\mathrm{rr}}^{(2g)\prime} \mathrm{T}_{\mathrm{ss}}^{(2g+2)\prime}}, \\ -\sqrt{\overline{\mathrm{T}}_{\mathrm{rr}}^{(2g)\prime} \overline{\mathrm{T}}_{\mathrm{ss}}^{(2g+2)\prime}} \leq 2\mathrm{A}_{\mathrm{rs}}^{2g+1} - \mathrm{T}_{\mathrm{rs}}^{(2g+1)} \quad & \leq \sqrt{\overline{\mathrm{T}}_{\mathrm{rr}}^{(2g)\prime} \overline{\mathrm{T}}_{\mathrm{ss}}^{(2g+2)\prime}}, \end{aligned} \tag{75}$$

where we used (24) to substitute for $\overline{\mathrm{T}}^{(2g+1)}$. The lower bound is not useful in the diagonal case when $g \geq 0$, and r = s, because then $\mathrm{T}_{\mathrm{rr}}^{(2g+1)} \geq 0$. Note that $\mathrm{A}_{\mathrm{rr}}^{2g+1} \geq 0$ for $g \geq 0$ is a graph theoretical quantity, and the products under the square root are non-negative. For off-diagonal moments, the quantity $\mathrm{T}_{\mathrm{rs}}^{(2g+1)}$ may take either sign.

10.2.2 CS bounds for even spectral moments

We can find bounds for even moments by replacing g with $g{-}1$, and h with $g{+}1$ in (69), (71) to give

$$| \mathrm{T}_{\mathrm{rs}}^{(2g)\prime} |^2 \leq \mathrm{T}_{\mathrm{rr}}^{(2g-2)\prime} \mathrm{T}_{\mathrm{ss}}^{(2g+2)\prime}, \quad | \overline{\mathrm{T}}_{\mathrm{rs}}^{(2g)\prime} |^2 \leq \overline{\mathrm{T}}_{\mathrm{rr}}^{(2g-2)\prime} \overline{\mathrm{T}}_{\mathrm{ss}}^{(2g+2)\prime}. \tag{76}$$

These bounds involve moments that step by ± 2 and are likely to be less accurate than the step-1 bounds defined in (73). However, we can recover *partial* step-1 bounds for even moments by using half-integral values in the definitions. If we use the power $g{+}\frac{1}{2}$ in the definition of x in (65) the

coefficients are real for positive eigenvalues, and imaginary for negative. It follows that the formula for the spectral moment is recovered only for *Aufbau* configurations with particle (electron) numbers in the range $0 \leq n_e \leq 2n_+ + 2\eta$, covering the non-negative eigenvalue spectrum. A similar modification to $\bar{x}$ in (70) leads to bounds for hole numbers in the range $0 \leq n_h \leq 2n_- + 2\eta$. Hence, subject to appropriate restrictions in electron/hole configuration, we have partial bounds

$$\begin{aligned} -\sqrt{\mathrm{T}_{\mathrm{rr}}^{(2g-1)}\mathrm{T}_{\mathrm{ss}}^{(2g+1)}} \leq & \quad \mathrm{T}_{\mathrm{rs}}^{(2g)\prime} \quad \leq \sqrt{\mathrm{T}_{\mathrm{rr}}^{(2g-1)}\mathrm{T}_{\mathrm{ss}}^{(2g+1)}}, \\ -\sqrt{\overline{\mathrm{T}}_{\mathrm{rr}}^{(2g-1)}\overline{\mathrm{T}}_{\mathrm{ss}}^{(2g+1)}} \leq & \quad \mathrm{T}_{\mathrm{rs}}^{(2g)\prime} - 2\mathrm{A}_{\mathrm{rs}}^{2g} \quad \leq \sqrt{\overline{\mathrm{T}}_{\mathrm{rr}}^{(2g-1)}\overline{\mathrm{T}}_{\mathrm{ss}}^{(2g+1)}}. \end{aligned} \tag{77}$$

Note that we have removed the primes have been removed from the odd spectral moments. Ranges of validity of these hole and particle expressions overlap, so that both expressions are effective in the region of $\mathcal{C}_{\mathrm{nat}}$.

10.2.3 CS bounds for charge and bond order

Bond order p_{rs} and charge $q_{\mathrm{r}} = p_{\mathrm{rr}}$ are $g = 0$ spectral moments, and have contributions from the nullspace, K. If we *allow* k∈K in (65) and set $g = h = 0$ in (68) we recover a bound quoted as a consequence of the CS inequality by Coulson and Longuet-Higgins as long ago as 1947 [10]:

$$|\, \mathrm{T}_{\mathrm{rs}}^{(0)} \,|^2 \leq \mathrm{T}_{\mathrm{rr}}^{(0)}\mathrm{T}_{\mathrm{ss}}^{(0)} \implies |\, p_{\mathrm{rs}} \,|^2 \leq q_{\mathrm{r}}q_{\mathrm{s}}, \tag{78}$$

which holds for all *Aufbau* configurations, and in particular implies the restriction of all bond orders at $\mathcal{C}_{\mathrm{nat}}$ for a bipartite graph to the range $[-1, 1]$. A similar formula including nullspace contributions can be derived for the hole bond order (see (30)) from (71)

$$|\, \overline{\mathrm{T}}_{\mathrm{rs}}^{(0)} \,|^2 \leq \overline{\mathrm{T}}_{\mathrm{rr}}^{(0)}\overline{\mathrm{T}}_{\mathrm{ss}}^{(0)} \implies |\, \bar{p}_{\mathrm{rs}} \,|^2 \leq (2 - q_{\mathrm{r}})(2 - q_{\mathrm{s}}) \tag{79}$$

The bounds described above relate bond order to charge, and by analogy with our previous moment bounds they are 'step 0'. We can also derive 'step 1' partial bounds in the manner that leads to (77). We are obliged to use the definitions of x and $\bar{x}$ that *exclude* nullspace contributions ((65) and (70)). We define

$$p'_{\mathrm{rs}} = p_{\mathrm{rs}} - p_{\mathrm{rs}}^{\mathrm{K}}, \quad \bar{p}'_{\mathrm{rs}} = \bar{p}_{\mathrm{rs}} - \bar{p}_{\mathrm{rs}}^{\mathrm{K}} \tag{80}$$

where the nullspace terms are

$$p^{\mathrm{K}}_{\mathrm{rs}} = \nu_{\mathrm{K}} \sum_{\mathrm{k}\in\mathrm{K}} \mathrm{U}_{\mathrm{rk}}\mathrm{U}^{*}_{\mathrm{sk}}, \quad \bar{p}^{\mathrm{K}}_{\mathrm{rs}} = \bar{\nu}_{\mathrm{K}} \sum_{\mathrm{k}\in\mathrm{K}} \mathrm{U}_{\mathrm{rk}}\mathrm{U}^{*}_{\mathrm{sk}}, \tag{81}$$

with $0 \leq \nu_{\mathrm{K}} \leq 2$ and $\bar{\nu}_{\mathrm{K}} = 2 - \nu_{\mathrm{K}}$. Using (65) and (70) with $g = 0$ gives

$$p'_{\mathrm{rs}} \leq \sqrt{\mathrm{T}^{(-1)}_{\mathrm{rr}}\mathrm{T}^{(1)}_{\mathrm{ss}}}, \quad \bar{p}'_{\mathrm{rs}} \leq \sqrt{\overline{\mathrm{T}}^{(-1)}_{\mathrm{rr}}\overline{\mathrm{T}}^{(1)}_{\mathrm{ss}}}, \tag{82}$$

where we recognise, as before, that the indices r and s can be exchanged on the right-hand side to give an alternative upper bound. We can recover the full quantity p_{rs} by adding back the nullspace contribution and hence

$$p_{\mathrm{rs}} \leq \sqrt{\mathrm{T}^{(-1)}_{\mathrm{rr}}\mathrm{T}^{(1)}_{\mathrm{ss}}} + p^{\mathrm{K}}_{\mathrm{rs}}, \quad \bar{p}_{\mathrm{rs}} \leq \sqrt{\overline{\mathrm{T}}^{(-1)}_{\mathrm{rr}}\overline{\mathrm{T}}^{(1)}_{\mathrm{ss}}} + \bar{p}^{\mathrm{K}}_{\mathrm{rs}}. \tag{83}$$

For $\mathrm{r}\neq\mathrm{s}$, $p^{\mathrm{K}}_{\mathrm{rs}}$ and its hole counterpart may be of either sign and will vanish if either vertex is a CFV, or they may vanish for symmetry reasons. Equivalent bounds for charge follow from $p_{\mathrm{rr}} = q_{\mathrm{r}}$. The bound for q_{r} in (83) suggest an interpretation for the otherwise mysterious quantity $\widetilde{\mathrm{T}}^{-1}_{\mathrm{rr}}$ in terms of core charge and bond number since $\widetilde{\mathrm{T}}^{1}_{\mathrm{rr}} = \widetilde{N}_{\mathrm{r}}$ when $\mathrm{A}_{\mathrm{rr}} = 0$, as

$$\widetilde{\mathrm{T}}^{(-1)}_{\mathrm{rr}} \geq (\widetilde{q}_{\mathrm{r}} - \widetilde{q}^{\mathrm{K}}_{\mathrm{r}})^2 / \widetilde{N}_{\mathrm{r}}. \tag{84}$$

10.2.4 Sharpness of CS bounds

There are circumstances in which the CS particle bounds in (75) and (77) become exact. For example, if λ_1 is the only positive eigenvalue, then

$$\mathrm{T}^{(g)}_{\mathrm{rr}} = \nu_1 \lambda_1^g |\mathrm{U}_{\mathrm{r}1}|^2 = \lambda_1^g q_{\mathrm{r}}, \tag{85}$$

where $\nu_1 = 0$, 1 or 2 depending on the configuration, and hence

$$\sqrt{\mathrm{T}^{(2g)}_{\mathrm{rr}}\mathrm{T}^{(2h)}_{\mathrm{rr}}} = \mathrm{T}^{(g+h)}_{\mathrm{rr}}, \tag{86}$$

for *Aufbau* configurations with $0 \leq n_e \leq 2n_+ + 2\eta$. This range of electron numbers includes $\mathcal{C}_{\mathrm{nat}}$. The exactness of all the square root particle bound formulae in such a case follows directly. In fact this argument works when $n_e \leq 2$ regardless of the number of positive eigenvalues, since in such a case the formula quoted in (85) also holds.

The connected graphs with exactly one positive eigenvalue are characterised by Smith's theorem [28]. The chemical graphs in this class are $\mathcal{S}, \{K_{1,1,2}\}$, where

$$\mathcal{S} = \{K_2, K_3, K_4, K_{1,2}, K_{1,3}, K_{2,2}, K_{2,3}, K_{3,3}\}. \tag{87}$$

The CS hole bounds in (75) and (77) are also exact for some graphs. In contrast with the Perron eigenvalue, λ_1, which is always non-degenerate for a connected graph, the smallest eigenvalue, λ_n, may be degenerate. However, if the graph has a single *eigenspace* (shell) with negative eigenvalue,

$$\overline{\mathrm{T}}_{\mathrm{rr}}^{(g)} = \nu_n \lambda_n^g \sum_{\lambda_\mathrm{k}=\lambda_n} |\mathrm{U}_{\mathrm{r}k}|^2 = \lambda_n^g \bar{q}_\mathrm{r},$$

for the range of hole numbers where no positive eigenvalues are occupied. In such a case, the spectral moment is an eigenvalue power multiplying a single MO shell invariant, and

$$\sqrt{\overline{\mathrm{T}}_{\mathrm{rr}}^{(2g)} \overline{\mathrm{T}}_{\mathrm{rr}}^{(2h)}} = \overline{\mathrm{T}}_{\mathrm{rr}}^{(g+h)}. \tag{88}$$

Chemical graphs with a single negative eigenspace include $\mathcal{S}$, together with the 5-cycle, the trigonal prism and the Petersen graph. Graphs in the set $\mathcal{S}$ have a single positive eigenvalue *and* a single negative eigenspace. It follows that the particle and hole bounds are *all* tight for these graphs for a range of electron numbers around $\mathcal{C}_{\mathrm{nat}}$.

10.3 Non-configurational bounds

We now derive some non-configurational (NC) bounds that are independent of electron number. We define positive functionals based on even powers of the eigenvalues with $g \in \mathbb{Z}$ and an arbitrary constant, b, as

$$\begin{aligned} D &= 2 \sum_{\mathrm{k}\in\mathrm{C}\setminus\mathrm{K}} (b-\lambda_\mathrm{k})^2 \lambda_\mathrm{k}^{2g} |\mathrm{U}_{\mathrm{rk}}|^2 + \nu_\mathrm{O} \sum_{\mathrm{k}\in\mathrm{O}\setminus\mathrm{K}} (b-\lambda_\mathrm{O})^2 \lambda_\mathrm{O}^{2g} |\mathrm{U}_{\mathrm{rk}}|^2 \geq 0 \\ \overline{D} &= 2 \sum_{\mathrm{k}\in\mathrm{V}\setminus\mathrm{K}} (b+\lambda_\mathrm{k})^2 \lambda_\mathrm{k}^{2g} |\mathrm{U}_{\mathrm{rk}}|^2 + (2-\nu_\mathrm{O}) \sum_{\mathrm{k}\in\mathrm{O}\setminus\mathrm{K}} (b+\lambda_\mathrm{O})^2 \lambda_\mathrm{O}^{2g} |\mathrm{U}_{\mathrm{rk}}|^2 \geq 0. \end{aligned} \tag{89}$$

Quadratic factors in (89) can be expanded, and using (22) and (23), and recognising the \K notation:

$$D = b^2 \mathrm{T}_{\mathrm{rr}}^{(2g)\prime} - 2b\mathrm{T}_{\mathrm{rr}}^{(2g+1)} + \mathrm{T}_{\mathrm{rr}}^{(2g+2)\prime} \geq 0,$$
$$\overline{D} = b^2 \overline{\mathrm{T}}_{\mathrm{rr}}^{(2g)\prime} + 2b\overline{\mathrm{T}}_{\mathrm{rr}}^{(2g+1)} + \overline{\mathrm{T}}_{\mathrm{rr}}^{(2g+2)\prime} \geq 0, \tag{90}$$

where we are able to omit the prime from the odd spectral moments. Using the normalisation condition, (24), we have

$$D^{\mathrm{sum}} = D + \overline{D} = 2b^2(\mathrm{A}_{\mathrm{rr}}^{2g})' + 4b\left[\mathrm{A}_{\mathrm{rr}}^{2g+1} - \mathrm{T}_{\mathrm{rr}}^{(2g+1)}\right] + 2(\mathrm{A}_{\mathrm{rr}}^{2g+2})' \geq 0, \tag{91}$$

where the primed terms are defined *via* (67) and (72) as

$$(\mathrm{A}_{\mathrm{rr}}^{2g})' = (\mathrm{T}_{\mathrm{rr}}^{(2g)\prime} + \overline{\mathrm{T}}_{\mathrm{rr}}^{(2g)\prime})/2 = \mathrm{A}_{\mathrm{rr}}^{2g} - \delta_{g0}\widetilde{q}_{\mathrm{r}}^{\mathrm{K}}. \tag{92}$$

After rearrangement (91) becomes

$$\mathrm{T}_{\mathrm{rr}}^{(2g+1)} \leq \mathrm{A}_{\mathrm{rr}}^{2g+1} + \frac{1}{2}\left[b(\mathrm{A}_{\mathrm{rr}}^{2g})' + \frac{1}{b}(\mathrm{A}_{\mathrm{rr}}^{2g+2})'\right] = B. \tag{93}$$

We can make the bound $B(b)$ stationary by setting

$$\frac{dB}{db} = \frac{1}{2}\left((\mathrm{A}_{\mathrm{rr}}^{2g})' - \frac{1}{b^2}(\mathrm{A}_{\mathrm{rr}}^{2g+2})'\right) = 0, \tag{94}$$

so that

$$(b^{\mathrm{opt}})^2 = (\mathrm{A}_{\mathrm{rr}}^{2g+2})'/(\mathrm{A}_{\mathrm{rr}}^{2g})', \tag{95}$$

and since

$$\frac{d^2B}{db^2} = (\mathrm{A}^{2g})'/b^3, \tag{96}$$

the choice of the positive square root in (95) leads to a minimum in B. Hence, the best *upper* bound of this type is

$$\mathrm{T}_{\mathrm{rr}}^{(2g+1)} \leq \mathrm{A}_{\mathrm{rr}}^{2g+1} + [(\mathrm{A}_{\mathrm{rr}}^{2g})'(\mathrm{A}_{\mathrm{rr}}^{2g+2})']^{\frac{1}{2}}. \tag{97}$$

There is no need for a corresponding bound for even moments, $\mathrm{T}_{\mathrm{rr}}^{(2g)}$, as they have ramp profiles with highest value $2\mathrm{A}_{\mathrm{rr}}^{2g}$ at $n_e{=}2n$ for every graph.

11 Results

Illustrative calculations are presented for some sample molecules. (See Fig. 3.) Each example is discussed in terms of the nature of the graph, the moment properties and their GS and CS and NC bounds. Results are presented in tabular form for $\mathcal{C}_{\rm nat}$, and graphical form for the full range of electron counts. Errors quoted in the tables are defined as percentage difference between bound and exact property values at $\mathcal{C}_{\rm nat}$; upper/lower bounds give positive/negative errors. Calculated spectral moments are shown in the graphs by solid lines marked with points at shell boundaries. All graphs have a vertical solid line marking $\mathcal{C}_{\rm nat}$. Partial particle bounds are plotted over the region from the empty π-system up to $\mathcal{C}_{\rm nat}$, and partial hole bounds from $\mathcal{C}_{\rm nat}$ to full.

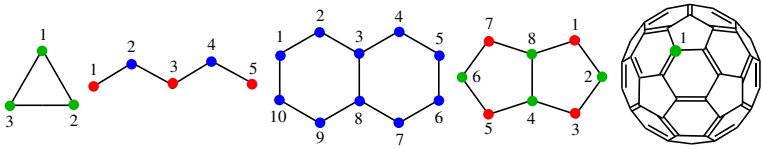

Figure 3. Molecules of interest: cyclopropenium, pentadiene, naphthalene, pentalene, C_{60}. Vertices: red for CV, green for CFV middle, blue for CFV upper; The numerical labels are used in Tables 1-10, and Figs. 4-12.

11.1 The cyclopropenium cation

At $\mathcal{C}_{\rm nat}$ cyclopropenium has a two-electron closed shell structure. The graph C_3 is non-bipartite, with all vertices CFV middle, and has nullity zero. Eigenvalues are $2, -1, -1$. The single positive and negative eigenspaces give rise to simple property profiles, and sharp GS ((59), (60)) and CS bounds ((75), (77)). Tables 1 and 2 illustrate the special status of C_3 (shared with all graphs in the set $\mathcal{S}$ (87)) with respect to bounds at $\mathcal{C}_{\rm nat}$. Spectral moments are shown in Fig. 4. Even moments have a ramp, odd moments a ziggurat profile. Odd moments satisfy $\mathrm{T}_{\rm rr}^{(2g-1)}=2\mathrm{A}_{\rm rr}^{2g-1}$ at $n_e=2n$, which is negative for $g<0$: $\mathrm{A}_{\rm rr}^{-1}=-1/2$, $\mathrm{A}_{\rm rr}^{-3}=-5/8$. Unlike GS and CS bounds, the NC bound is not sharp, as C_3 is not a star.

g	r	Type	GSpu	%	GShu	%	$T_{rr}^{(g)}$	GSpl	%	GShl	%
-2	1	CFV	0.1667	0	0.1667	0	**0.1667**	0.1667	0	0.1667	0
-1	1	CFV	0.3333	0	0.3333	0	**0.3333**	0.3333	0	0.3333	0
1	1	CFV	1.3333	0	1.3333	0	**1.3333**	1.3333	0	1.3333	0
2	1	CFV	2.6667	0	2.6667	0	**2.6667**	2.6667	0	2.6667	0

Table 1. $T_{rr}^{(g)}$ for cyclopropenium at $\mathcal{C}_{nat}$ with GS bounds.

g	r	Type	CSp	%	$T_{rr}^{(g)}$	CSh	%	NC	%
-2	1	CFV	0.1667	0	**0.1667**	0.1667	0	-	-
-1	1	CFV	0.3333	0	**0.3333**	0.3333	0	0.3660	10
0	1	CFV	0.6667	0	**0.6667**	0.6667	0	-	-
1	1	CFV	1.3333	0	**1.3333**	1.3333	0	1.4142	6
2	1	CFV	2.6667	0	**2.6667**	2.6667	0	-	-

Table 2. $T_{rr}^{(g)}$ for cyclopropenium at $\mathcal{C}_{nat}$ with CSp and CSh bounds, and NC bounds for g odd.

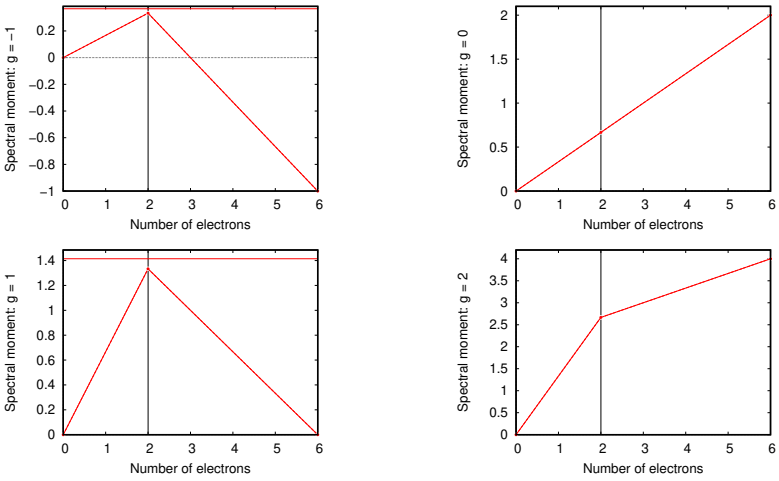

Figure 4. $T_{rr}^{(g)}$ for cyclopropenium. Particle and hole GS and CS bounds coincide with exact values. Solid horizontal lines mark the NC bound.

11.2 The pentadiene molecule

Pentadiene has graph P_5, which is bipartite with eigenvalues $\sqrt{3}, 1, 0, -1, -\sqrt{3}$, hence $\eta = 1$. Vertices 1, 3 and 5 are CV, and 2 and 4 are CFV upper (see Fig. 3). There are 5 π-electrons at $\mathcal{C}_{\rm nat}$. Exact spectral moments are shown in Fig. 5 and Fig. 6. Results for vertices 1, 2 and 3 are shown in red, blue and magenta, respectively.

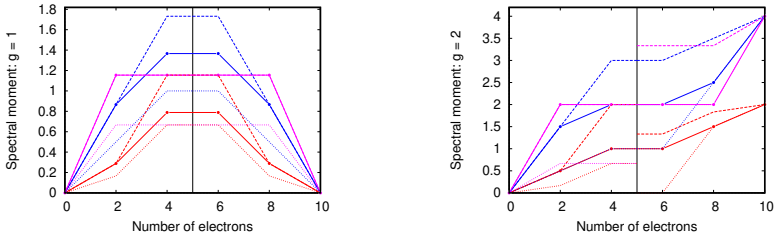

Figure 5. $\mathrm{T}_{\rm rr}^{(g)}$ for pentadiene (solid): vertex 1 (red), 2 (blue), and 3 (magenta), with GS upper (dashed) and lower bounds (dotted).

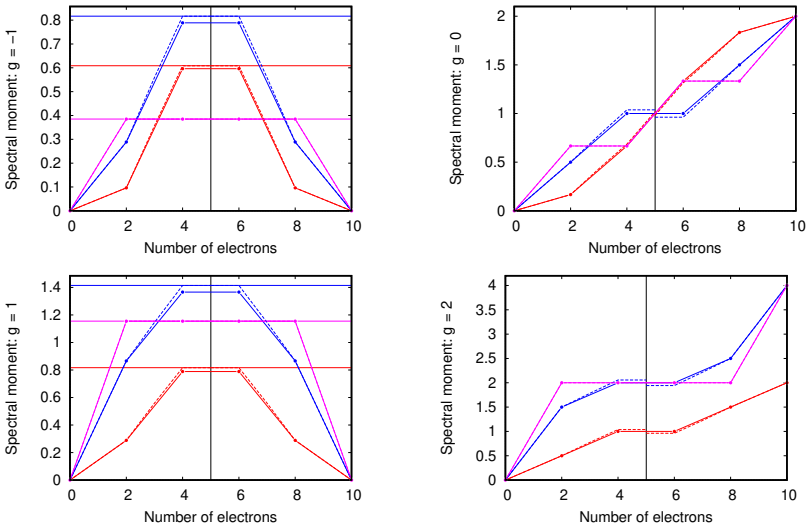

Figure 6. $\mathrm{T}_{\rm rr}^{(g)}$ for pentadiene (solid): vertex 1 (red), 2 (blue), and 3 (magenta), with CS (dashed), and NC (horizontal) bounds.

The straight line segments arise from the filling of individual shells (eigenspaces), and change gradient when a new shell starts to fill. For $g = 0$ the exact moments all show zero gradient where the nullspace is being filled ($4 \leq n_e \leq 6$), for the obvious reasons that for $g > 0$, $\lambda^{\mathrm{K}} = 0$, and for $g < 0$ the nullspace is excluded from the sum. The charge, $\mathrm{T}_{\mathrm{rr}}^{(0)}$, however, has non-zero gradient in this range for vertices 1 and 3 because they are CV, and zero gradient for vertex 2, as it is a CFV. More subtly, vertex 3 has zero gradient for all moments for $2 \leq n_e \leq 8$, as both MOs 2 and 4 have a node through the central vertex; in other words, because vertex 3 is both λ_2-CFV and λ_4-CFV. Table 3 shows spectral moments and

g	r	Type	GSpu	%	GShu	%	$\mathrm{T}_{\mathrm{rr}}^{(g)}$	GSpl	%	GShl	%
-2	1	CV	0.6667	20	0.8889	60	**0.5556**	0.2222	-60	0.4444	-20
	2	CFV	1.0000	50	1.0000	50	**0.6667**	0.3333	-50	0.3333	-50
	3	CV	0.6667	200	0.2222	0	**0.2222**	0.2222	0	-0.2222	-200
-1	1	CV	0.6667	12	0.6667	12	**0.5962**	0.3849	-35	0.3849	-35
	2	CFV	1.0000	27	1.0000	27	**0.7887**	0.5774	-27	0.5774	-27
	3	CV	0.6667	73	0.6667	73	**0.3849**	0.3849	0	0.3849	0
1	1	CV	1.1547	46	1.1547	46	**0.7887**	0.6667	-15	0.6667	-15
	2	CFV	1.7321	27	1.7321	27	**1.3660**	1.0000	-27	1.0000	-27
	3	CV	1.1547	0	1.1547	0	**1.1547**	0.6667	-42	0.6667	-42
2	1	CV	2.0000	100	1.3333	33	**1.0000**	0.6667	-33	0.0000	-100
	2	CFV	3.0000	50	3.0000	50	**2.0000**	1.0000	-50	1.0000	-50
	3	CV	2.0000	0	3.3333	67	**2.0000**	0.6667	-67	2.0000	0

Table 3. $\mathrm{T}_{\mathrm{rr}}^{(g)}$ for pentadiene at $\mathcal{C}_{\mathrm{nat}}$ with GS bounds.

GS bounds at $\mathcal{C}_{\mathrm{nat}}$, while Fig. 5 shows the same quantities over the whole range of electron numbers. The upper bound GS errors for CV are very large, but much smaller for CFV. The GS bounds show odd/even effects with g values. For odd moments, particle and hole upper bounds coincide at $\mathcal{C}_{\mathrm{nat}}$, as do the particle and hole lower bounds. For even moments the particle upper and hole lower bounds have identical errors but with opposite sign, as do the particle lower and hole upper bounds. Both of these observations follow from the pairing theorem. The GS particle upper bounds for the central vertex, 3, are special because they have zero errors for all $g > 0$. This is again because of the λ_2-CFV status of the vertex. The Perron eigenvector is the unique positive eigenspace with weight on vertex 3, and the bounds are exact. The fourth MO also has a node passing

g	r	Type	CSp	%	$\mathrm{T}_{\mathrm{rr}}^{(g)}$	CSh	%	NC	%
-2	1	CV	0.5632	1	**0.5556**	0.5479	-1	-	-
	2	CFV	0.6857	3	**0.6667**	0.6476	-3	-	-
	3	CV	0.2222	0	**0.2222**	0.2222	0	-	-
-1	1	CV	0.6086	2	**0.5962**	0.6086	2	0.6086	2
	2	CFV	0.8165	4	**0.7887**	0.8165	4	0.8165	4
	3	CV	0.3849	0	**0.3849**	0.3849	0	0.3849	0
0	1	CV	1.0191	2	**1.0000**	0.9809	-2	-	-
	2	CFV	1.0380	4	**1.0000**	0.9620	-4	-	-
	3	CV	1.0000	0	**1.0000**	1.0000	0	-	-
1	1	CV	0.8165	4	**0.7887**	0.8165	4	0.8165	4
	2	CFV	1.4142	4	**1.3660**	1.4142	4	1.4142	4
	3	CV	1.1547	0	**1.1547**	1.1547	0	1.1547	0
2	1	CV	1.0380	4	**1.0000**	0.9620	-4	-	-
	2	CFV	2.0572	3	**2.0000**	1.9428	-3	-	-
	3	CV	2.0000	0	**2.0000**	2.0000	0	-	-

Table 4. $\mathrm{T}_{\mathrm{rr}}^{(g)}$ for pentadiene at $\mathcal{C}_{\mathrm{nat}}$ with CSp, CSh and NC bounds.

through vertex 3, so for a similar reason, the even-g hole upper and odd-g hole lower bounds are exact. Table 4 shows the CS bounds at $\mathcal{C}_{\mathrm{nat}}$, whilst Fig. 6 shows the same quantities over the whole range of electron numbers. The errors in the bounds are very small, and they show the same odd/even behaviour exhibited in the GS case. The central vertex has zero errors for the same reasons as before.

Note that the NC bound gives stronger results here than the Coulson-Moffitt bound (43) since $q_{\mathrm{r}}^{\mathrm{K}}$ is not zero. In fact, for vertex 3 it is exact as this vertex participates in only one positive and one negative eigenspace. Vertex 1, as the terminal vertex of a path, is λ_{k}-CV for all five eigenvalues and its NC bound is therefore not exact. The same logic applies to moments $\mathrm{T}_{\mathrm{rr}}^{(-1)}$.

11.3 The naphthalene molecule

Naphthalene has a bipartite molecular graph with $\eta = 0$, and hence 5 positive and 5 negative eigenvalues, which are $\pm(1+\sqrt{13})/2$, $\pm(1+\sqrt{5})/2$, $\pm(\sqrt{13}-1)/2$, ±1, $\pm(\sqrt{5}-1)/2$. All vertices are CFV upper, and the unique vertices, 1, 2 and 3 (see Fig. 3) are respectively at ring shoulder, ring apex and ring junction. At $\mathcal{C}_{\mathrm{nat}}$ naphthalene has a 10 π closed-shell configuration. Vertex 1 is of type λ_{k}-CV in all eigenvectors; vertex 2 is

of type λ_k-CFV in the HOMO-1, λ_k-CV otherwise; vertex 3 is λ_k-CFV for LOMO+1 and HOMO, and λ_k-CV otherwise. Exact spectral moments are shown as functions of electron number in Fig. 7 and Fig. 8. The

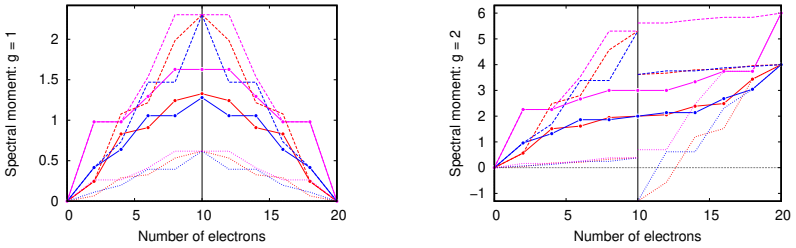

Figure 7. $T_{rr}^{(g)}$ for naphthalene (solid): vertex 1 (red), 2 (blue), and 3 (magenta) with GS upper (dashed) and lower (dotted) bounds.

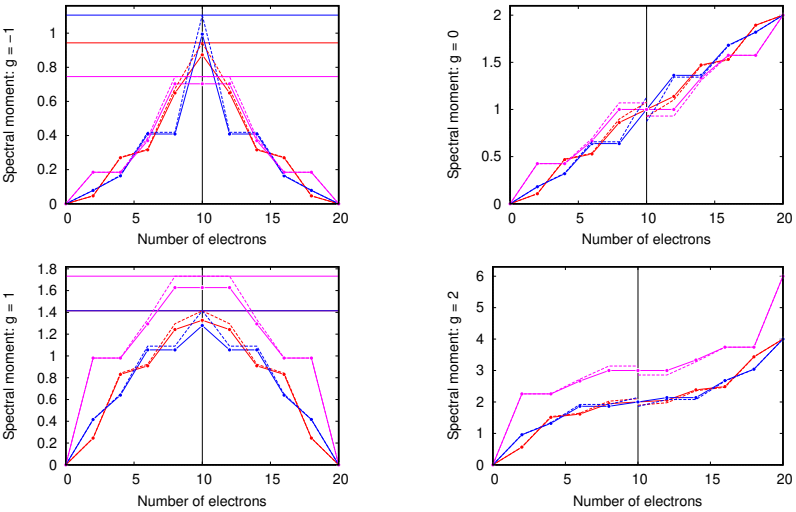

Figure 8. $T_{rr}^{(g)}$ for naphthalene (solid): vertex 1 (red), 2 (blue), and 3 (magenta) with CS (dashed), and NC (solid horizontal) bounds.

respective ziggurat and ramp profiles, the flat steps and function limits all follow from the vertex types. The molecular graph is unweighted and bipartite, so particle and hole partial bounds meet for all vertices at $\mathcal{C}_{\mathrm{nat}}$

in Fig. 7 (left) as they depend only on eigenvalues. In Fig. 7 (right), on the particle side, upper and lower bounds are independent of vertex at $\mathcal{C}_{\rm nat}$. The hole bounds, however, are derived from bounds on $\overline{\rm T}_{\rm rr}^{(2)}$ so there is a jump at $\mathcal{C}_{\rm nat}$ and different values for vertices of different degree (see (24)). GS bounds for $\rm T_{rr}^{(g)}$ at $\mathcal{C}_{\rm nat}$ are not exact, and show large errors, as to be expected for a graph with many eigenvalues different from λ_1. For *all* odd values of g all GS upper bounds are identical. GS lower bounds are also equal, again as follows from the bipartite non-singular nature of the graph.

In contrast, the CS bounds are accurate at $\mathcal{C}_{\rm nat}$ (Table 6) and over the

g	r	Type	GSpu	%	GShu	%	$\rm T_{rr}^{(g)}$	GSpl	%	GShl	%
-2	1	CFV	2.6180	195	1.5892	79	**0.8889**	0.1886	-79	-0.8403	-195
	2	CFV	2.6180	114	2.2559	85	**1.2222**	0.1886	-85	-0.1736	-114
	3	CFV	2.6180	371	0.9225	66	**0.5556**	0.1886	-66	-1.5069	-371
-1	1	CFV	1.6180	85	1.6180	85	**0.8730**	0.4343	-50	0.4343	-50
	2	CFV	1.6180	63	1.6180	63	**0.9944**	0.4343	-56	0.4343	-56
	3	CFV	1.6180	130	1.6180	130	**0.7031**	0.4343	-38	0.4343	-38
1	1	CFV	2.3028	73	2.3028	73	**1.3277**	0.6180	-53	0.6180	-53
	2	CFV	2.3028	80	2.3028	80	**1.2793**	0.6180	-52	0.6180	-52
	3	CFV	2.3028	41	2.3028	41	**1.6276**	0.6180	-62	0.6180	-62
2	1	CFV	5.3028	165	3.6180	81	**2.0000**	0.3820	-81	-1.3028	-165
	2	CFV	5.3028	165	3.6180	81	**2.0000**	0.3820	-81	-1.3028	-165
	3	CFV	5.3028	77	5.6180	87	**3.0000**	0.3820	-87	0.6972	-77

Table 5. $\rm T_{rr}^{(g)}$ for naphthalene at $\mathcal{C}_{\rm nat}$ with GS bounds.

g	r	Type	CSp	%	$\rm T_{rr}^{(g)}$	CSh	%	NC	%
-2	1	CFV	0.9529	7	**0.8889**	0.8249	-7	-	-
	2	CFV	1.3095	7	**1.2222**	1.1349	-7	-	-
	3	CFV	0.5792	4	**0.5556**	0.5319	-4	-	-
-1	1	CFV	0.9428	8	**0.8730**	0.9428	8	0.9428	8
	2	CFV	1.1055	11	**0.9944**	1.1055	11	1.1055	11
	3	CFV	0.7454	6	**0.7031**	0.7454	6	0.7454	6
0	1	CFV	1.0766	8	**1.0000**	0.9234	-8	-	-
	2	CFV	1.1279	13	**1.0000**	0.8721	-13	-	-
	3	CFV	1.0698	7	**1.0000**	0.9302	-7	-	-
1	1	CFV	1.4142	7	**1.3277**	1.4142	7	1.4142	7
	2	CFV	1.4142	11	**1.2793**	1.4142	11	1.4142	11
	3	CFV	1.7321	6	**1.6276**	1.7321	6	1.7321	6
2	1	CFV	2.1032	5	**2.0000**	1.8968	-5	-	-
	2	CFV	2.1409	7	**2.0000**	1.8591	-7	-	-
	3	CFV	3.1420	5	**3.0000**	2.8580	-5	-	-

Table 6. $\rm T_{rr}^{(g)}$ for naphthalene at $\mathcal{C}_{\rm nat}$ with CSp, CSh and NC bounds.

range of electron number (see Fig. 8). For odd moments, CSp and CSh are both upper bounds that meet at $\mathcal{C}_{\rm nat}$, whilst for even g the particle and hole expressions give upper and lower bounds, respectively with equal and opposite errors. Exactness of CS bounds for $n_e \leq 2$ and $n_h \leq 2g_{\rm HUMO}$ is found for all graphs (see §10.2.4), and persists here to $n_e \leq 4$ for vertex 3 because of its λ_2-CFV status.

11.4 The pentalene molecule

Pentalene has a non-bipartite molecular graph with $\eta = 1$, four positive and three negative eigenvalues (3.2429, $\sqrt{2}$, 1, 0.4708, 0, $-\sqrt{2}$, -1.8136, and -2). At $\mathcal{C}_{\rm nat}$ there are 9 π-electrons and a singly-occupied nullspace. Vertex (1) is CV, and vertices 2 and 4 are CFV middle (see Fig. 3).

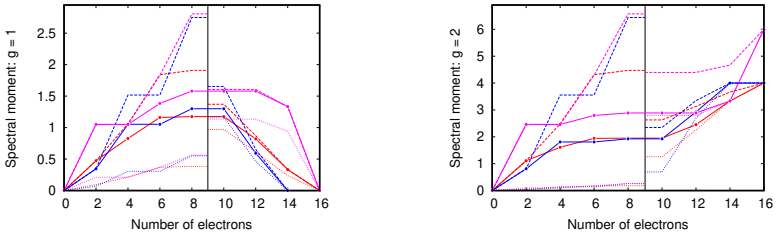

Figure 9. $\mathrm{T}_{\rm rr}^{(g)}$ for pentalene (solid): vertex 1 (red), 2 (blue), and 4 (magent) with GSp (dashed)and GSh (dotted) bounds.

g	r	Type	GSpu	%	GShu	%	$\mathrm{T}_{\rm rr}^{(g)}$	GSpl	%	GShl	%
-2	1	CV	3.6770	487	0.7037	12	**0.6266**	0.1484	-76	0.5323	-15
	2	CFV	5.2956	100	2.7933	5	**2.6506**	0.2137	-92	2.5866	-2
	4	CFV	5.4055	136	2.2994	0	**2.2921**	0.2182	-90	2.0988	-8
-1	1	CV	1.7307	163	0.7346	12	**0.6583**	0.3477	-47	0.5927	-10
	2	CFV	2.4926	63	1.5846	3	**1.5337**	0.5007	-67	1.4134	-8
	4	CFV	2.5443	81	1.5674	11	**1.4082**	0.5111	-64	1.4012	0
1	1	CV	1.9086	63	1.3708	17	**1.1742**	0.3834	-67	0.9693	-17
	2	CFV	2.7487	111	1.6536	27	**1.2998**	0.5522	-58	1.1693	-10
	4	CFV	2.8058	78	1.6049	2	**1.5796**	0.5637	-64	1.1348	-28
2	1	CV	4.4717	129	2.6292	35	**1.9495**	0.1805	-91	1.2585	-35
	2	CFV	6.4401	235	2.3464	22	**1.9251**	0.2599	-86	0.6928	-64
	4	CFV	6.5737	128	4.3951	52	**2.8867**	0.2653	-91	2.7902	-3

Table 7. $\mathrm{T}_{\rm rr}^{(g)}$ for pentalene at $\mathcal{C}_{\rm nat}$ with GS bounds.

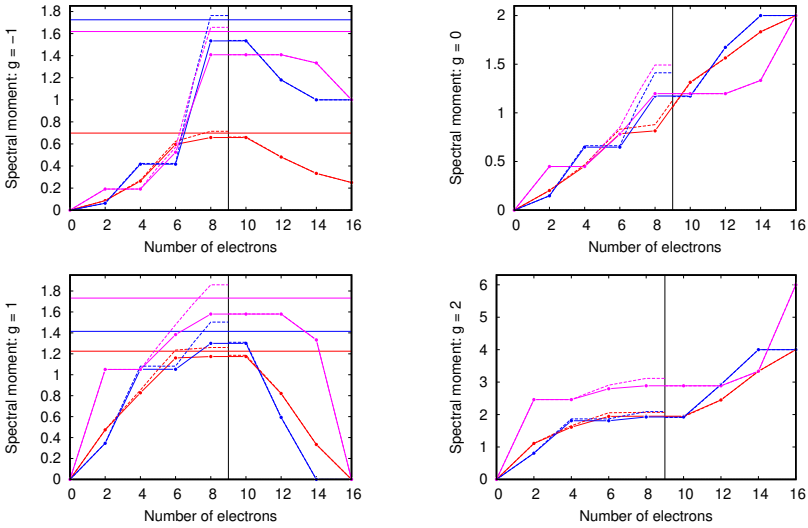

Figure 10. $T_{rr}^{(g)}$ for pentalene (solid): vertex 1 (red), 2 (blue), and 4 (magenta) with CSp and CSu (dashed), and NC bounds (solid horizontal).

g	r	Type	CSp	%	$T_{rr}^{(g)}$	CSh	%	NC	%
-2	1	CV	0.6869	10	**0.6266**	0.6240	0	-	-
	2	CFV	2.8326	7	**2.6506**	2.6484	0	-	-
	4	CFV	2.4767	8	**2.2921**	2.2919	0	-	-
-1	1	CV	0.7145	9	**0.6583**	0.6626	1	0.6978	6
	2	CFV	1.7635	15	**1.5337**	1.5374	0	1.7247	12
	4	CFV	1.6568	18	**1.4082**	1.4085	0	1.6180	15
0	1	CV	1.1292	6	**1.0646**	1.0576	-1	-	-
	2	CFV	1.4119	20	**1.1732**	1.1671	-1	-	-
	4	CFV	1.4914	25	**1.1976**	1.1970	0	-	-
1	1	CV	1.2602	7	**1.1742**	1.1855	1	1.2247	4
	2	CFV	1.5029	16	**1.2998**	1.3098	1	1.4142	9
	4	CFV	1.8593	18	**1.5796**	1.5806	0	1.7321	10
2	1	CV	2.0684	6	**1.9495**	1.9316	-1	-	-
	2	CFV	2.0909	9	**1.9251**	1.9091	-1	-	-
	4	CFV	3.1151	8	**2.8867**	2.8849	0	-	-

Table 8. $T_{rr}^{(g)}$ for pentalene at $\mathcal{C}_{nat}$ with CSp, CSh and NC bounds.

All three are λ_k-CFV for some λ_k (vertex 1 is CFV for k $= 4, 5, 6$, vertex 2 for k $= 2, 4, 8$, and vertex 4 for $\lambda_k = 2, 5, 6$), which leads to multiple flat features, including the final zero at $n_e = 14$ for the bond number of vertex 2 in Fig. 9 (left), and Fig. 10 (bottom left). As the graph is non-bipartite, the profiles are not symmetrical, and do not have a meeting of corresponding particle and hole bounds. Again, GS bounds give large errors (Table 7), with hole bounds performing better, as might be expected for a molecule with more positive than negative eigenvalues. The greater accuracy of the hole bounds carries over into the CS bounds shown in Table 8, where the errors are at the 1% level or smaller. NC bounds for bond number simply repeat the Coulson-Moffitt bound ($\sqrt{d_r}$) for CFV vertices 2 and 4, but improve on it for CV vertex 1.

11.5 The C_{60} molecule

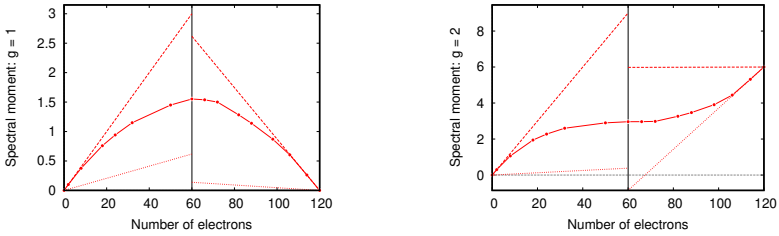

Figure 11. $T_{rr}^{(g)}$ for C_{60} (solid) with GS upper (dashed) and lower (dotted) bounds.

C_{60} has a non-bipartite graph that is 3-regular and vertex transitive with all vertices CFV middle. The 60 MOs correspond to fewer distinct eigenvalues, as I_h symmetry confers degenerate eigenspaces. As a leapfrog fullerene, the neutral has a closed shell with $\eta = 0$; hence, by transitivity $\widetilde{q}_r = 1$. Exact spectral moments over the range are plotted in Fig. 11 and Fig. 12. By transitivity, all vertices are λ_k-CV for all k, so there are no flat steps. GS bounds are shown in Table 9 at $\mathcal{C}_{nat}$, and over the range in Fig. 11. Errors are large, as C_{60} with its large Perron eigenvalue and high number of eigenvalues is a bad case for GS bounds. Table 10 shows modest errors for CS particle bounds and CS hole bounds for $g > 0$.

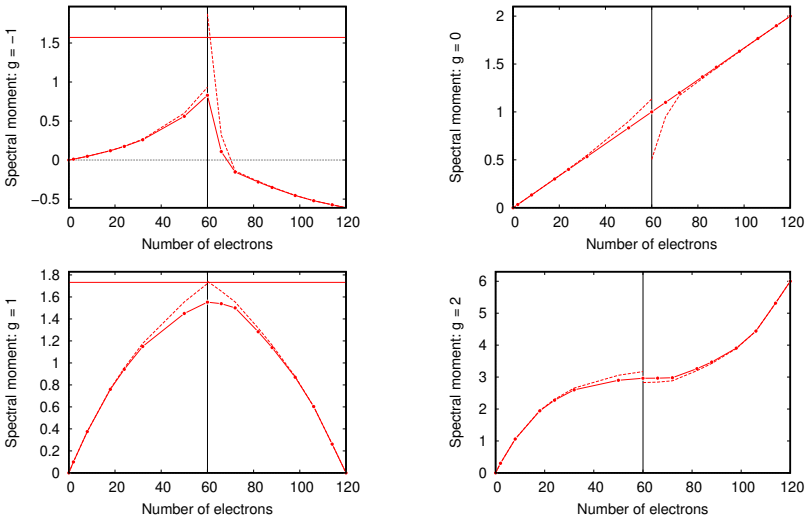

Figure 12. $T_{rr}^{(g)}$ for C_{60} (solid) with CS (dashed), and NC (horizontal) bounds.

g	r	Type	GSpu	%	GShu	%	$T_{rr}^{(g)}$	GSpl	%	GShl	%
-2	1	CFV	2.6180	201	6.8958	693	**0.8695**	0.1111	-87	-45.0415	-5280
-1	1	CFV	1.6180	95	6.6058	696	**0.8298**	0.3333	-60	-0.2291	-128
1	1	CFV	3.0000	93	2.6180	69	**1.5527**	0.6180	-60	0.1386	-91
2	1	CFV	9.0000	204	5.9808	102	**2.9638**	0.3820	-87	-0.8541	-129

Table 9. $T_{rr}^{(g)}$ for C_{60} at $\mathcal{C}_{nat}$ with GS bounds.

g	r	Type	CSp	%	$T_{rr}^{(g)}$	CSh	%	NC	%
-2	1	CFV	0.9454	9	**0.8695**	-0.5083	-158	-	-
-1	1	CFV	0.9325	12	**0.8298**	1.8733	126	1.5708	89
0	1	CFV	1.1351	14	**1.0000**	0.5043	-50	-	-
1	1	CFV	1.7216	11	**1.5527**	1.7425	12	1.7321	12
2	1	CFV	3.1720	7	**2.9638**	2.8280	-5	-	-

Table 10. $T_{rr}^{(g)}$ for C_{60} at $\mathcal{C}_{nat}$ with CSp, CSh and NC bounds.

11.6 Bond order profiles

Property profiles for diagonal spectral moments follow the standard ziggurat and ramp profiles for naphthalene and pentalene, albeit with loss of

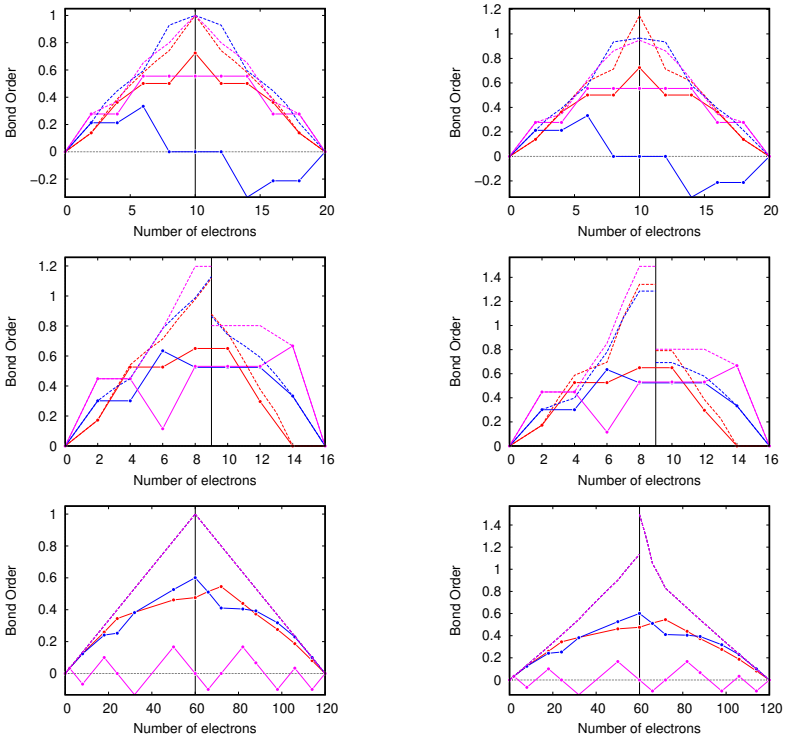

Figure 13. Bond order profiles (solid) for naphthalene, pentalene and C_{60} in rows 1, 2 and 3: vertex pairs (red, blue and magenta, respectively) are 1-2, 1-3 and 3-8 (naphthalene), 1-2, 1-8 and 4-8 (pentalene), and hex-pent, hex-hex and apex-apex (C_{60}). CS particle and hole bounds (dashed) are from equations (78,79) (column 1), and (83) (column 2).

symmetry in the pentalene case. The bond order, $p_{\rm rs}$, as an off-diagonal matrix element, can show the more varied profiles of the third kind. Fig. 13 shows bond order profiles for a selection of vertex pairs in napthalene, pentalene and C_{60}. As naphthalene has a bipartite molecular graph, profiles are symmetric in electron count for edge bond orders (and for all pairs of centres in different partite sets), but antisymmetric for pairs in the same partite set (*e.g.* the blue line in row 1). This follows from the pairing the-

orem and the fact that the gradient of $p_{\rm rs}$ as a given shell is filled depends on the size and sign of a shell invariant for the $\lambda_{\rm k}$ eigenspace, *i.e.*

$$\sum_{\lambda_{\rm k'}=\lambda_{\rm k}} {\rm U}_{\rm rk'}{\rm U}^*_{\rm sk'}.$$

For a flat segment to appear it is sufficient that one of r and s is a $\lambda_{\rm k}$-CFV. Bond order for the non-bonded pair rs $= 1, 3$ shows the strongest variation, with a swing from net bonding to net anti-bonding and eventual cancellation as the π-manifold fills up. Non-bipartite pentalene shows less symmetrical behaviour, as expected.

The profiles for C_{60} are undramatic for edge bonds; flat segments are absent for this vertex-transitive graph. Plots for pent-hex and hex-hex bonds show the familiar inversion from a strong Fries-like structure of the neutral to the Clar-like structure of the 12-anion as the 6 low lying LUMOs characteristic of a leapfrog fullerene fill [16]. Bond order associated with antipodal pairs of vertices varies strongly, as demanded by g or u character of the shells, and it vanishes identically at some intermediate fillings.

For off-diagonal spectral moments such as $p_{\rm rs}$ there is a subtlety. For diagonal spectral moments it was clear that we could dispense with the negative branch in (77). For off-diagonal spectral moments it is not possible *a priori* to predict the sign of the property outside the initial 2 π-electron segment and in principle both branches of the CS square root bound apply.

12 Conclusions

This paper presents a variety of bounds to general spectral moments. These can be found as equations (53), (54) (GSO/GS particle bounds) in §10.1.2, as (58) (GSO hole bounds) in §10.1.3, as (59)-(62)(GS *and* GSO bounds at $\mathcal{C}_{\rm nat}$) in §10.1.4, as (75), (77) (CS bounds) in §10.2, and as (97)(non-configurational bounds) in §10.3. The bounds are probably of most interest when specialised to the basic properties of charge, bond order and bond number. In this final section of the paper we convert the general expressions to ready-to-use form for these properties in the natural configuration. Note that the GS bounds are eigenvalue based and hence

of relevance only to bond number, as are our non-configurational bounds, whereas the CS bounds apply also to charge and bond order.

For *bond order* we note (§10.2.3) that a CS argument recovers the well-known bound connecting bond order and charge [10]

$$(\mathcal{C}_{\rm nat}: \text{all}) \qquad |\,\widetilde{p}_{\rm rs}\,|^2 \leq q_{\rm r} q_{\rm s}, \tag{98}$$

and its less remarked hole version

$$(\mathcal{C}_{\rm nat}: \text{all}) \qquad |\,\widetilde{p}_{\rm rs}\,|^2 \leq (2-q_{\rm r})(2-q_{\rm s}), \tag{99}$$

both of which for bipartite graphs reduce to

$$(\mathcal{C}_{\rm nat}: \text{bip}) \qquad |\,\widetilde{p}_{\rm rs}\,|^2 \leq 1. \tag{100}$$

By taking a version of the CS derivation that excludes nullspace contributions, we found an intriguing bound relating core charge and bond number to the otherwise apparently nebulous spectral moment of order -1, *i.e.*

$$\widetilde{\rm T}_{\rm rr}^{(-1)} \geq (\widetilde{q}_{\rm r} - \widetilde{q}_{\rm r}^{\rm K})^2 / \widetilde{N}_{\rm r}. \tag{101}$$

For *bond number*, Gutman-style particle bounds (GS and GSO) are

$$(\mathcal{C}_{\rm nat}\text{: CV: all}) \qquad \lambda_+(\widetilde{q}_{\rm r} - \widetilde{q}_{\rm r}^{\rm K}) \leq \widetilde{N}_{\rm rr} \leq \lambda_1(\widetilde{q}_{\rm r} - \widetilde{q}_{\rm r}^{\rm K}). \tag{102}$$

$$(\mathcal{C}_{\rm nat}\text{: CFV: all}) \qquad \lambda_+ \widetilde{q}_{\rm r} \leq \widetilde{N}_{\rm rr} \leq \lambda_1 \widetilde{q}_{\rm r}. \tag{103}$$

and the hole bounds for unweighted graphs are

$$(\mathcal{C}_{\rm nat}\text{: CV: all}) \qquad -\lambda_n(2 - \widetilde{q}_{\rm r} - \widetilde{q}_{\rm r}^{\rm K}) \geq \widetilde{N}_{\rm rr} \geq -\lambda_-(2 - \widetilde{q}_{\rm r} - \widetilde{q}_{\rm r}^{\rm K}), \tag{104}$$

$$(\mathcal{C}_{\rm nat}\text{: CFV: all}) \qquad -\lambda_n(2 - \widetilde{q}_{\rm r}) \geq \widetilde{N}_{\rm rr} \geq -\lambda_-(2 - \widetilde{q}_{\rm r}), \tag{105}$$

Particle and hole bounds reduce to single expressions for bipartite graphs:

$$(\mathcal{C}_{\rm nat}\text{: CV: bip}) \qquad -\lambda_+(1 - \widetilde{q}_{\rm r}^{\rm K}) \leq \widetilde{N}_{\rm rr} \leq -\lambda_1(1 - \widetilde{q}_{\rm r}^{\rm K}), \tag{106}$$

$$(\mathcal{C}_{\rm nat}\text{: CFV: bip}) \qquad \lambda_+ \leq \widetilde{N}_{\rm rr} \leq \lambda_1, \tag{107}$$

since $\lambda_1 = -\lambda_n$ and $\lambda_+ = -\lambda_-$. As noted earlier, bounds in (102), (103) become sharp for all vertices of molecular graphs with exactly one positive eigenvalue (such as the star) and similarly in (104), (105) are sharp for all vertices of molecular graphs with one negative eigenspace.

CS particle bounds for bond number follow from (74) as

$$(\mathcal{C}_{\rm nat}\text{: all}) \qquad (\widetilde{N}_{\rm r})^2 \leq (\widetilde{q}_{\rm r} - \widetilde{q}_{\rm r}^{\rm K})\widetilde{\rm T}_{\rm rr}^{(2)}, \tag{108}$$

and in the hole case

$$(\mathcal{C}_{\rm nat}\text{: all}) \qquad (\widetilde{N}_{\rm r})^2 \leq (2 - \widetilde{q}_{\rm r} - \widetilde{q}_{\rm r}^{\rm K})(2d_{\rm r} - \widetilde{\rm T}_{\rm rr}^{(2)}), \tag{109}$$

reducing for bipartite graphs to

$$(\mathcal{C}_{\rm nat}\text{: bip}) \qquad (\widetilde{N}_{\rm r})^2 \leq (1 - \widetilde{q}_{\rm r}^{\rm K})d_{\rm r}, \tag{110}$$

which for a CV in a bipartite graph is a tighter bound than the simple Coulson-Moffitt (CM) $d_{\rm r}$ [17], since $0 \leq \widetilde{q}_{\rm r}^{\rm K} < 1$. CM is attained *only* for the central vertex of the star, which is a CFV; (110) is also an equality for CFV vertices of the star. Bounds (108) and (109) can be tighter than CM for some vertices in some graphs depending on the detailed behaviour of $\widetilde{\rm T}_{\rm rr}^{(2)}$. Other cases for which they are exact are discussed in §10.2.4.

Finally, the NC bound for general spectral moments in (97) translates to a relation between bond number and charge,

$$E_{\rm r}^{\pi} = N_{\rm r} + {\rm A}_{\rm rr}q_{\rm r} \leq {\rm A}_{\rm rr} + \sqrt{(1 - \widetilde{q}_{\rm r}^{\rm K}){\rm A}_{\rm rr}^2}. \tag{111}$$

which for unweighted bipartite or non-bipartite graphs reduces to

$$(\mathcal{C}_{\rm nat}\text{: all}) \qquad \widetilde{N}_{\rm r} \leq \sqrt{(1 - \widetilde{q}_{\rm r}^{\rm K})d_{\rm r}} \leq \sqrt{d_{\rm r}}. \tag{112}$$

This constitutes a strengthening of the Coulson-Moffitt bound for CVs.

***Acknowledgment*:** PWF thanks the Leverhulme Trust for an Emeritus Fellowship 'Modelling Molecular Currents and Aromaticity', and the Master and Fellows of Peterhouse, Cambridge for a Visiting Fellowship.

References

[1] A. Bjerhammar, Rectangular reciprocal matrices, with special reference to geodetic calculations, *Bull. Géodésique (1946-1975)* **20** (1951) 188–220.

[2] J. K. Burdett, S. Lee, Moments and the energies of solids, *J. Am. Chem. Soc* **107** (1985) 3050–3063.

[3] J. K. Burdett, S. Lee, W. Sha, The method of moments and the energy levels of molecules and solids, *Croat. Chim. Acta* **57** (1984) 1193–1216.

[4] J. K. Burdett, J. F. Mitchell, Order–disorder transitions and the method of moments, *J. Chem. Phys.* **102** (1995) 6757–6761.

[5] F. H. Burkitt, C. A. Coulson, H. C. Longuet-Higgins, Free valence in unsaturated hydrocarbons, *Trans. Faraday Soc.* **47** (1951) 553–564.

[6] A. Cauchy, *Analyse Algébrique, Cours d'Analyse de l'École Royale Polytechnique, Ire Partie*, Paris 1821.

[7] A. Ceulemans, E. Lijnen, P. W. Fowler, R. B. Mallion, T. Pisanski, Graph theory and the Jahn-Teller theorem, *Proc. Roy. Soc. A* **468** (2012) 971–989.

[8] B. H. Chirgwin, C. A. Coulson, J. T. Randall, The electronic structure of conjugated systems. VI, *Proc. R. Soc. A* **201** (1950) 196–209.

[9] C. A. Coulson, Free valence in organic reactions, *J. Chim. Phys. Phys. Chim. Biol.* **45** (1948) 247–248.

[10] C. A. Coulson, H. C. Longuet-Higgins, The electronic structure of conjugated systems I. General theory, *Proc. R. Soc. A* **191** (1947) 39–60.

[11] C. A. Coulson, H. C. Longuet-Higgins, The electronic structure of conjugated systems II. Unsaturated hydrocarbons and their hetero-derivatives, *Proc. R. Soc. A* **192** (1947) 16–32.

[12] C. A. Coulson, H. C. Longuet-Higgins, The electronic structure of conjugated systems III. Bond orders in unsaturated molecules, *Proc. R. Soc. A* **194** (1948) 447–456.

[13] C. A. Coulson, H. C. Longuet-Higgins, The electronic structure of conjugated systems IV. Force constants in unsaturated hydrocarbons, *Proc. R. Soc. A* **193** (1948) 453–464.

[14] C. A. Coulson, H. C. Longuet-Higgins, The electronic structure of conjugated systems V. The interaction of two conjugated systems, *Proc. R. Soc. A* **195** (1949) 188–197.

[15] E. Estrada, M. Benzi, What is the meaning of the graph energy after all? *Discr. Appl. Math.* **230** (2017) 71–77.

[16] P. W. Fowler, A. Ceulemans, Electron deficiency of the fullerenes, *J. Phys. Chem.* **99** (1995) 508–510.

[17] P. W. Fowler, B. T. Pickup, In search of Coulson's lost theorem, *J. Chem. Phys.* **151** (2019) #151101.

[18] I. Gutman, Bounds for reactivity indices, *Theor. Chim. Acta* **47** (1978) 217–222.

[19] D. R. Hartree, The wave mechanics of an atom with a non-Coulomb central field. Part I. Theory and methods, *Math. Proc. Cambridge Phil. Soc.* **24** (1928) 89–110.

[20] X. Li, Y. Shi, I. Gutman, *Graph Energy*, Springer, New York, 2012.

[21] S. Marković, I. Gutman, Spectral moments of the edge adjacency matrix in molecular graphs. Benzenoid hydrocarbons, *J. Chem Inf. Comput. Sci.* **39** (1999) 289–293.

[22] B. J. McClelland, Properties of the latent roots of a matrix: the estimation of π-electron energies, *J. Chem. Phys.* **54** (2003) 640–643.

[23] E. H. Moore, On the reciprocal of the general algebraic matrix, *Bull. Am. Math. Soc.* **26** (1920) 394–395.

[24] R. Penrose, A generalized inverse for matrices, *Math. Proc. Cambridge Philos. Soc.* **51** (1955) 406–413.

[25] I. Sciriha, On the coefficient of λ in the characteristic polynomial of singular graphs, *Util. Math.* **52** (1997) 97–111.

[26] I. Sciriha, On the construction of graphs of nullity one, *Discr. Math.* **181** (1998) 193–211.

[27] J. C. Slater, *Quantum Theory of Molecules and Solids. Volume 2: Symmetry and Energy Bands in Crystals*, McGraw-Hill, New York, 1965.

[28] J. H. Smith, Some properties of the spectrum of a graph, in: R. Guy, H. Hanani, N. Sauer, J. Schönheim (Eds.), *Combinatorial Structures and their Applications*, Gordon & Breach, Philadelphia, 1970, pp. 403–406.

[29] M. Steele, *The Cauchy-Schwarz Masterclass: An Introduction to Mathematical Inequalities*, Cambridge Univ. Press, Cambridge, 2004.

[30] Y. Tsuji, E. Estrada, R. Movassagh, R. Hoffmann, Quantum interference, graphs, walks, and polynomials, *Chem. Rev.* **118** (2018) 4887–4911.